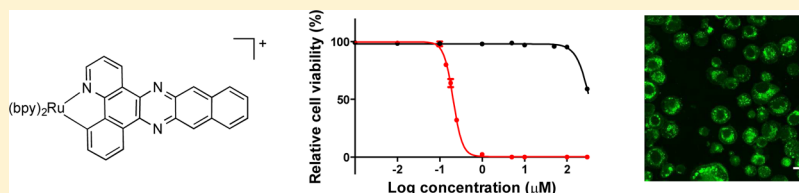


Organometallic Ru(II) Photosensitizers Derived from π -Expansive Cyclometalating Ligands: Surprising Theranostic PDT Effects

Tariq Sainuddin, Julia McCain, Mitch Pinto, Huimin Yin, Jordan Gibson, Marc Hetu, and Sherri A. McFarland*

Department of Chemistry, Acadia University, Wolfville, Nova Scotia B4P 2R6, Canada

S Supporting Information



ABSTRACT: The purpose of the present study was to investigate the influence of π -expansive cyclometalating ligands on the photophysical and photobiological properties of organometallic Ru(II) compounds. Four compounds with increasing π conjugation on the cyclometalating ligand were prepared, and their structures were confirmed by HPLC, 1D and 2D ^1H NMR, and mass spectrometry. The properties of these compounds differed substantially from their Ru(II) polypyridyl counterparts. Namely, they were characterized by red-shifted absorption, very weak to no room temperature phosphorescence, extremely short phosphorescence state lifetimes (<10 ns), low singlet oxygen quantum yields (0.5–8%), and efficient ligand-centered fluorescence. Three of the metal complexes were very cytotoxic to cancer cells in the dark (EC_{50} values = 1–2 μM), in agreement with what has traditionally been observed for Ru(II) compounds derived from small $\text{C}^{\wedge}\text{N}$ ligands. Surprisingly, the complex derived from the most π -expansive cyclometalating ligand exhibited no cytotoxicity in the dark ($\text{EC}_{50} > 300$ μM) but was phototoxic to cells in the nanomolar regime. Exceptionally large phototherapeutic margins, exceeding 3 orders of magnitude in some cases, were accompanied by bright ligand-centered intracellular fluorescence in cancer cells. Thus, Ru(II) organometallic systems derived from π -expansive cyclometalating ligands, such as 4,9,16-triazadibenzo[*a,c*]naphthacene (pbpn), represent the first class of potent light-responsive Ru(II) cyclometalating agents with theranostic potential.

1. INTRODUCTION

Ru(II) polypyridyl complexes have been widely studied for more than 30 years due to their attractive photophysical and electrochemical properties. Their utility has been explored across a variety of technological areas: dye-sensitized solar cells,¹ solar fuels photochemistry,² light-emitting electrochemical cells,³ photoluminescence sensors,⁴ biophotonics,⁵ photochromics,⁶ water-oxidation catalysts,⁷ water-reduction catalysts,⁸ low-power photon upconversion,⁹ and in more fundamental studies of photoinduced electron and energy transfer.¹⁰ More recently, Ru(II) polypyridyl complexes have been investigated as light-responsive agents in a range of photobiological applications—namely as mediators of photodynamic therapy (PDT) or photoactivated cancer therapy (PACT),^{11–23} and as covalent modifiers of DNA in photochemotherapy (PCT).^{24–30} A 2015 review by Knoll and Turro highlights some of the most recent and important contributions related to phototoxic Ru(II) polypyridyl complexes.²⁸

By comparison, the related class of cyclometalated Ru(II) complexes has received very little focus over the same time period. Fewer than 20 $[\text{Ru}(\text{LL})_2(\text{C}^{\wedge}\text{N})]^+$ complexes appear in the Cambridge Structural Database as of 2015, and these are based on $\text{C}^{\wedge}\text{N} = \text{phpy}^-$ (deprotonated 2-phenylpyridine) or derivatives of phpy^- .^{31,32} This lack of attention may stem, in

part, from the very short excited state lifetimes that characterize the cyclometalated systems,³³ which are generally up to 2 orders of magnitude shorter than the hallmark 1 μs lifetime of the prototype $[\text{Ru}(\text{bpy})_3]^{2+}$ ($\text{bpy} = 2,2'$ -bipyridine) complex.¹⁰ The strong σ -donating capacities of cyclometalating ligands, such as phpy^- , raise the energy of the metal-based $d\pi$ HOMO orbitals to a greater extent than the diimine-based LUMOs, leading to unusually low-energy triplet metal-to-ligand charge transfer (MLCT) excited states that are governed by the energy gap law. The ensuing poor photoluminescence and attenuated metal-based oxidation potentials have limited the utility of cyclometalated Ru(II) complexes as luminescent sensors and as sensitizers in other photonic applications. Similarly, Turro and co-workers noted that cyclometalated complexes do not appear to be good candidates for the design of new PCT agents that operate via photoinduced ligand substitution,³⁴ presumably due to the increased energy required to reach dissociative triplet metal-centered (MC) states that would otherwise undergo ligand substitution to form covalent DNA adducts. Nevertheless, their characteristic robustness and red-shifted absorption relative to the analogous polypyridyl systems has prompted

Received: August 17, 2015

Published: December 16, 2015

continued effort toward adapting these structures for use as panchromatic light-harvesting sensitizers for a variety of light-based applications.^{35–37}

An additional challenge to the development of coordinatively saturated tris-bidentate cyclometalated Ru(II) complexes as light-responsive prodrugs, lies in their inherent cytotoxicity, which is often significantly greater than that of the well-known anticancer drug cisplatin.^{36–38} High dark cytotoxicities compounded by modest light cytotoxicities have produced suboptimal phototherapeutic margins of less than 10-fold for this class of organometallic Ru(II) systems to date.³⁶ Similar to the parent $[\text{Ru}(\text{bpy})_2(\text{phpy}^-)]^+$, all of these compounds appear to possess lowest-energy $^3\text{MLCT}$ states with pure $\text{Ru} \rightarrow$ diimine character and derive from a similar scaffold: a cyclometalating phpy^- or benzo[*h*]quinoline (bhq^-) ancillary ligand combined with diimine coligands, such as bpy, 2,2'-biquinoline (biq), [1,10]phenanthroline[5,6]dione, or benzo[*i*]dipyrido[3,2-*a*:2',3'-*c*]phenazine (dppn).

To the best of our knowledge, cyclometalation with π -expansive ligands that could serve as the site of excited-state charge localization (or reduction) has not been explored. We hypothesized that such systems might combine the best attributes of cyclometalated Ru(II) complexes (thermal stability with broad, low-energy absorption into the PDT window) and polypyridyl Ru(II) metal–organic dyads (potent PDT effects with low dark cytotoxicities) and be particularly well-suited for use as PDT agents. Herein, we report that certain π -expansive cyclometalating ligands do, in fact, turn cytotoxic organometallic Ru(II) complexes into attractive photosensitizers for PDT (or PACT) (compounds 1–4, Chart 1) and highlight that the number of fused rings is critical.

Chart 1. Cyclometalated Ru(II) Complexes Investigated in this Study and the Labeling Used for ^1H NMR Assignments

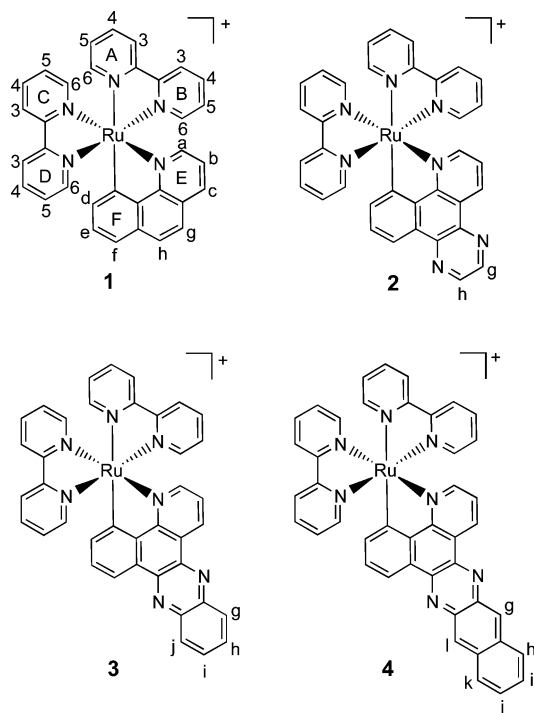
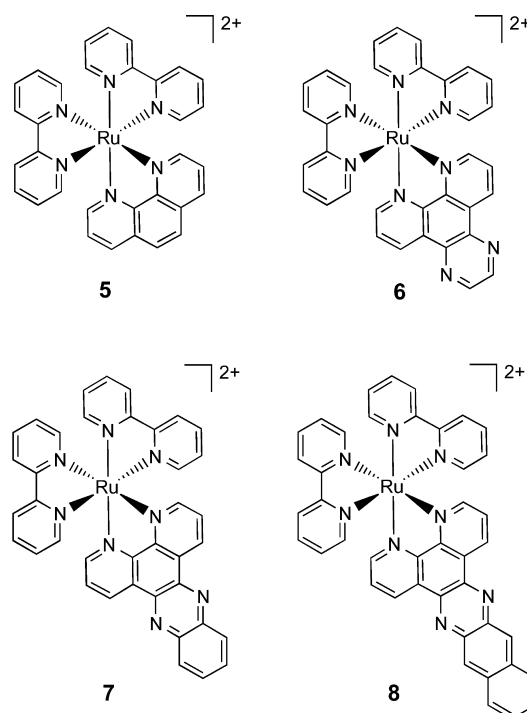


Chart 2. Ru(II) Polypyridyl Complexes Used as Reference Compounds in this Study



2. EXPERIMENTAL PROCEDURES

2.1. Materials. 2,2'-Bipyridine (bpy), 2,3-diaminonaphthalene, benzo[*h*]quinoline (bhq), and $\text{RuCl}_3 \cdot x\text{H}_2\text{O}$ were purchased from Sigma-Aldrich and used without further purification. $[\text{Ru}(\text{bpy})_2\text{Cl}_2] \cdot 2\text{H}_2\text{O}$ was prepared by an established procedure.³⁹ Characterized fetal bovine serum (FBS) (VWR), RPMI 1640 (Corning Cellgro), and Eagle's Minimum Essential Medium (EMEM) (Corning Cellgro) were purchased from VWR. Human promyelocytic leukemia cells (HL-60) and human malignant melanoma cells (SK-MEL-28) were procured from the American Type Culture Collection. Prior to use, FBS was divided into 40 mL aliquots that were heat inactivated (30 min, 55 °C) and subsequently stored at –20 °C. Water for biological experiments was deionized to a resistivity of 18 M Ω cm using a Barnstead filtration system.

2.2. Instrumentation. Microwave reactions were performed in a CEM Discover microwave reactor. NMR spectra were collected using Bruker AVANCE 500 (Dalhousie University Nuclear Magnetic Resonance Research Resource) or 300 (Acadia Centre for Microstructural Analysis) MHz spectrometers, and ESI mass spectra were obtained using a Bruker microTOF focus mass spectrometer (Dalhousie University Mass Spectrometry Laboratory). HPLC analyses were carried out on an Agilent/Hewlett-Packard 1100 series instrument (ChemStation Rev. A. 10.02 software) using a Hypersil GOLD C18 reversed-phase column with an A-B gradient (98% \rightarrow 40% A; A = 0.1% formic acid in H_2O , B = 0.1% formic acid in MeOH). Reported retention times are correct to within ± 0.1 min.

2.3. Synthesis. The preparation and characterization of compound 1 has been previously reported but using a different synthetic method.³³ Reference polypyridyl Ru(II) compounds 5–8 were synthesized according to modified literature protocols reported previously^{15,40–43} using microwave irradiation at 180 °C for 10 min and characterized by TLC, ^1H NMR, and mass spectrometry. The metal complexes for this study were isolated and purified as PF_6^- salts and subsequently subjected to anion metathesis on Amberlite IRA-410 with MeOH to yield the more water-soluble Cl^- salts for biological experiments. ^1H NMR and electrospray ionization ESI (+ve) mass spectra were collected on PF_6^- salts in $\text{MeCN-}d$ and MeCN, respectively.

Benzo[h]quinoline (bhq). ^1H NMR (500 MHz, chloroform-*d*): δ 9.33 (dd, $J = 8.3, 1.3$ Hz, 1H, x), 9.02 (dd, $J = 4.4, 1.7$ Hz, 1H, a), 8.18 (dd, $J = 8.0, 1.9$ Hz, 1H, c), 7.91 (d, $J = 7.8$ Hz, 1H, g), 7.82 (d, $J = 8.8$ Hz, 1H, f), 7.76 (ddd, $J = 8.3, 6.9, 1.5$ Hz, 1H, d), 7.72 (dd, $J = 7.7, 1.4$ Hz, 1H, h), 7.70–7.66 (m, 1H, e), 7.53 (dd, $J = 8.0, 4.2$ Hz, 1H, b). HPLC retention time: 31.598 min, 33.842 min. TLC of commercial bhq showed 4 spots (1% MeOH:CH₂Cl₂).

Benzo[h]quinoline-5,6-dione. Benzo[h]quinoline-5,6-dione was synthesized following a literature method.⁴⁴ Benzo[h]quinoline (3.6 g, 20 mmol) and iodopentoxide (8.2 g, 25 mmol) were added to a 250 mL round-bottom flask with glacial acetic acid (50 mL). The orange mixture was heated at reflux (118 °C) for 3 h, resulting in a dark purple solution. The reaction was determined to have gone to completion by ^1H NMR spectroscopy. The product was precipitated by the addition of deionized water (~75 mL) and left to stand overnight at room temperature. The precipitate was isolated by vacuum filtration using a medium glass-sintered frit and subsequently dissolved in chloroform (300 mL) to give a dark red solution that was washed with 100 mL of sat. NaHCO₃ and 100 mL of sat. Na₂S₂O₃. The organic layer was dried with anhydrous Na₂SO₄, and the solvent was removed by rotary evaporation to give a dark brown solid (4.1 g, 97%). $R_f = 0.22$ (10% EtOAc in hexanes). ^1H NMR (300 MHz, chloroform-*d*): δ 8.92 (dd, $J = 4.7, 1.9$ Hz, 1H, a), 8.73 (ddd, $J = 7.9, 1.3, 0.6$ Hz, 1H, x), 8.43 (dd, $J = 7.9, 1.9$ Hz, 1H, c), 8.23 (ddd, $J = 7.8, 1.4, 0.6$ Hz, 1H, f), 7.83 (ddd, $J = 7.9, 7.4, 1.4$ Hz, 1H, d), 7.61 (td, $J = 7.6, 1.2$ Hz, 1H, e), 7.45 (dd, $J = 7.9, 4.7$ Hz, 1H, b). HPLC retention time: 24.30 min.

4,9,12-Triazadibenzo[a,c]naphthalene (pbpq). Pbpq was synthesized using a procedure adapted from the literature.⁴⁵ Benzo[h]quinoline-5,6-dione (209 mg, 1.0 mmol) was added to a 100 mL round-bottom flask with methanol (30 mL). Ethylene diamine (67 mg, 1.1 mmol) was added dropwise to the round-bottom flask, resulting in an orange solution that was heated at reflux (65 °C) for 4.5 h. The reaction was then cooled to room temperature, concentrated to 3 mL by rotary evaporation, and left to stand at 4 °C overnight. The resulting precipitate was removed by vacuum filtration, and a yellow powder was isolated from the filtrate by rotary evaporation. The product was purified by silica gel chromatography with 10% EtOAc in hexanes to yield a yellow powder (69 mg, 30%). $R_f = 0.68$ (30% EtOAc in hexanes). ^1H NMR (500 MHz, chloroform-*d*): δ 9.57 (d, $J = 6.0$ Hz, 1H, a), 9.44 (d, $J = 5.4$ Hz, 1H, x), 9.24 (d, $J = 6.9$ Hz, 1H, f), 9.17 (d, $J = 4.5$ Hz, 1H, c), 9.00 (d, $J = 2.0$ Hz, 1H, g), 8.95 (d, $J = 2.1$ Hz, 1H, h), 7.97–7.87 (m, 2H, d, e), 7.80–7.74 (m, 1H, b). HPLC retention time: 22.99, 28.26, 32.18 min.

4,9,14-Triazadibenzo[a,c]anthracene (pbpz). Benzo[h]quinoline-5,6-dione (174 mg, 0.83 mmol) and *o*-phenylenediamine (101 mg, 0.93 mmol) were combined in 30 mL of ethanol. The orange mixture was heated at reflux (78 °C) for 4 h, resulting in a dark red solution. The mixture was cooled to room temperature, and the resulting precipitate was vacuum filtered with a medium glass-sintered frit and washed with 50 mL of cold deionized water, 50 mL of cold ethanol, and 100 mL of cold diethyl ether to give a pale yellow powder (114 mg, 49%). $R_f = 0.63$ (30% EtOAc in hexanes). ^1H NMR (500 MHz, chloroform-*d*): δ 9.62 (dd, $J = 8.1, 1.8$ Hz, 1H, a), 9.39 (dd, $J = 7.8, 1.7$ Hz, 1H, x), 9.26 (dd, $J = 7.7, 1.6$ Hz, 1H, f), 9.09 (dd, $J = 4.4, 1.8$ Hz, 1H, c), 8.40–8.31 (m, 2H, h, i), 7.93–7.85 (m, 4H, d, e, i, j), 7.70 (dd, $J = 8.0, 4.5$ Hz, 1H, b). HPLC retention time: 26.70 min.

4,9,16-Triazadibenzo[a,c]naphthacene (pbpn). Pbpn was synthesized according to a procedure adapted from a literature preparation of 3-pyrid-2'-yl-4,9,16-triazadibenzo[a,c]naphthacene (pyHdbn).⁴⁶ Benzo[h]quinoline-5,6-dione (209 mg, 1.00 mmol) and 2,3-diaminonaphthalene (177 mg, 1.12 mmol) were added to a 100 mL round-bottom flask with ethanol (30 mL). The orange mixture was heated at reflux (78 °C) for 4.5 h, resulting in a dark red mixture. The mixture was cooled to room temperature, and the resulting precipitate was vacuum filtered with a fine glass-sintered frit and washed with 50 mL of cold deionized water, 50 mL of cold ethanol, and 100 mL of cold diethyl ether to give a brown powder (221 mg, 67%). $R_f = 0.36$ (10% EtOAc in hexanes). ^1H NMR (300 MHz, chloroform-*d*): δ 9.64 (d, $J = 7.9$ Hz, 1H, a), 9.43–9.36 (m, 1H, x), 9.24 (d, $J = 7.4$ Hz, 1H,

f), 9.08 (dd, $J = 4.6, 1.8$ Hz, 1H, c), 8.96 (s, 1H, g), 8.93 (s, 1H, l), 8.25–8.15 (m, 2H, h, k), 7.94–7.83 (m, 2H, d, e), 7.71 (dd, $J = 8.1, 4.6$ Hz, 1H, b), 7.66–7.58 (m, 2H, i, j). HPLC retention time: 34.02 min.

[Ru(bpy)₂(bhq)]PF₆ (1). [Ru(bpy)₂(bhq)]PF₆ was synthesized using an adapted literature procedure.⁴⁷ Ru(bpy)₂Cl₂·2H₂O (100 mg, 0.19 mmol) and bhq (37 mg, 0.21 mmol) were added to a microwave vessel containing triethylamine (1 mL) and ethylene glycol (3 mL). The mixture was subjected to microwave irradiation at 120 °C for 40 min. TLC indicated that not enough Ru(bpy)₂Cl₂·2H₂O had been added to consume the bhq ligand; thus, additional Ru(bpy)₂Cl₂·2H₂O (20 mg, 0.04 mmol) was added to the mixture, and it was microwaved for an additional 20 min at 120 °C. The purple mixture was pipetted into approximately 30 mL of stirring saturated KPF₆ solution. The resulting precipitate was vacuum filtered with a fine glass-sintered frit and purified by silica gel column chromatography with 5% H₂O and 0.5% sat. KNO₃ in MeCN to yield a mixture of PF₆⁻ and NO₃⁻ salts. The resulting solid was dissolved in 5–10 mL of water, and 1–2 mL of sat. KPF₆ was added to precipitate the desired PF₆⁻ salt. Subsequent extraction of the aqueous solution with dichloromethane and concentration under reduced pressure gave the pure PF₆⁻ salt as a purple solid (40 mg, 26%). $R_f = 0.73$ (10% H₂O + 2.5% sat. KNO₃ in MeCN). ^1H NMR (500 MHz, MeCN-*d*₃): δ 8.48 (dd, $J = 8.26, 1.18$ Hz, 1H, 3A), 8.39–8.32 (m, 2H, 3B, 3C), 8.29 (d, $J = 8.1$ Hz, 1H, 3D), 8.20 (dd, $J = 8.0, 1.4$ Hz, 1H, c), 8.04–7.96 (m, 2H, 4A, 6A), 7.91–7.77 (m, 5H, 4B, 6B, 6C, a, g), 7.76–7.67 (m, 3H, 4C, 4D, h), 7.63 (d, $J = 5.8$ Hz, 1H, 6D), 7.52–7.45 (m, 1H, 5A), 7.42 (d, $J = 7.8$ Hz, 1H, f), 7.33–7.19 (m, 3H, 5B, b, e), 7.04–7.08 (m, 2H, 5C, 5D), 6.69 (dd, $J = 7.0, 1.0$ Hz, 1H, d). MS (ESI+) m/z 592.2 [M – PF₆]⁺. HRMS ESI+ m/z for C₃₃H₂₄N₅Ru: calcd 592.1070, found 592.1060. HPLC retention time: 26.05 min.

[Ru(bpy)₂(pbpq)]PF₆ (2). [Ru(bpy)₂(pbpq)]PF₆ was synthesized using an adapted literature procedure.⁴⁷ Ru(bpy)₂Cl₂·2H₂O (135 mg, 0.26 mmol) and pbpq (46 mg, 0.20 mmol) were added to a microwave vessel containing triethylamine (1 mL) and ethylene glycol (3 mL). The mixture was subjected to microwave irradiation at 120 °C for 1 h and then pipetted into approximately 30 mL of stirring saturated KPF₆ solution. The resulting precipitate was vacuum filtered with a fine glass-sintered frit and purified by silica gel column chromatography with 10% MeOH in DCM. TLC indicated impurities in the purified product (62 mg), so the column was repeated with 1% MeOH in DCM to give a single spot by TLC. Purple solid (40 mg, 25%). $R_f = 0.69$ (10% H₂O + 2.5% sat. KNO₃ in MeCN). ^1H NMR (500 MHz, MeCN-*d*₃): δ 9.21 (dd, $J = 8.1, 1.4$ Hz, 1H, c), 9.00 (d, $J = 2.1$ Hz, 1H, g), 8.94 (d, $J = 2.1$ Hz, 1H, h), 8.50 (d, $J = 8.2$ Hz, 1H, 3A), 8.47 (dd, $J = 8.0, 1.0$ Hz, 1H, f), 8.41–8.36 (m, 2H, 3B, 3C), 8.32 (dd, $J = 9.0, 1.3$ Hz, 1H, 3D), 8.04 (td, $J = 7.9, 1.6$ Hz, 1H, 4A), 8.02–7.94 (m, 3H, 6A, 6C, a), 7.91–7.84 (m, 2H, 4B, 6B), 7.79–7.72 (m, 3H, 4C, 4D, 6D), 7.48 (ddd, $J = 7.5, 5.4, 1.2$ Hz, 1H, 5A), 7.43 (dd, $J = 8.1, 5.3$ Hz, 1H, b), 7.36 (t, $J = 7.5$ Hz, 1H, e), 7.29 (ddd, $J = 7.3, 5.7, 1.4$ Hz, 1H, 5B), 7.09–7.02 (m, 2H, 5C, 5D), 6.87 (dd, $J = 7.1, 1.0$ Hz, 1H, d). ¹³C NMR (75 MHz, CD₃CN): δ 187.38, 155.62, 154.76, 154.59, 153.96, 153.60, 152.29, 151.11, 148.54, 147.27, 147.09, 146.17, 141.63, 140.35, 139.99, 138.91, 136.81, 133.31, 132.70, 131.88, 130.87, 130.61, 128.22, 128.01, 125.52, 123.76, 123.09, 122.93, 122.73, 122.15, 120.16, 120.01, 119.74, 119.09, 112.75. MS (ESI+) m/z : 644.2 [M – PF₆]⁺. HRMS ESI+ m/z for C₃₃H₂₄N₅Ru: calcd 644.1131, found 644.1159. HPLC retention time: 26.46 min.

[Ru(bpy)₂(pbpz)]PF₆ (3). [Ru(bpy)₂(pbpz)]PF₆ was synthesized using an adapted literature procedure.⁴⁷ Ru(bpy)₂Cl₂·2H₂O (135 mg, 0.26 mmol) and pbpz (56 mg, 0.20 mmol) were added to a microwave vessel containing a mixture of triethylamine (1 mL) and ethylene glycol (3 mL). The purple solution was subjected to microwave irradiation at 120 °C for 1 h and then pipetted into 30 mL of a stirring saturated KPF₆ solution. The resulting precipitate was vacuum filtered with a fine glass-sintered frit and purified by silica gel column chromatography (5% MeOH:DCM). Purple solid (41 mg, 25%). $R_f = 0.70$ (10% H₂O + 2.5% sat. KNO₃ in MeCN). ^1H NMR (500 MHz, MeCN-*d*₃): δ 9.33 (dd, $J = 8.0, 1.5$ Hz, 1H, c), 8.61 (dd, $J = 7.8, 1.1$ Hz, 1H, f), 8.51 (d, $J = 8.2, 1.1$ Hz, 1H, 3A), 8.44–8.37 (m, 2H, 3B,

3C), 8.37–8.31 (m, 3H, 3D, g, j), 8.07–8.02 (m, 2H, 4A, 6C), 8.01–7.93 (m, 4H, 6A, a, h, i), 7.91–7.85 (m, 2H, 4B, 6B), 7.82 (d, $J = 5.7$, 1H, 6D), 7.78–7.75 (m, 2H, 4C, 4D), 7.48 (ddd, $J = 7.7$, 5.4, 1.2 Hz, 1H, 5A), 7.44 (dd, $J = 8.0$, 5.4 Hz, 1H, b), 7.36 (t, $J = 7.5$ Hz, 1H, e), 7.29 (ddd, $J = 7.4$, 5.6, 1.4 Hz, 1H, 5B), 7.12–7.07 (m, 2H, 5C, 5D), 6.88 (dd, $J = 7.2$, 1.1 Hz, 1H, d). ^{13}C NMR (75 MHz, CD_3CN): δ 187.90, 157.25, 154.61, 154.15, 153.96, 153.63, 152.45, 152.29, 152.18, 151.18, 148.95, 147.35, 147.08, 146.17, 140.77, 139.27, 138.43, 138.21, 133.66, 133.33, 131.93, 130.91, 130.67, 128.60, 128.29, 127.40, 126.90, 126.04, 126.00, 125.66, 123.78, 123.11, 122.98, 122.77, 120.19, 120.02, 119.77, 119.31, 113.66. MS (ESI+) m/z 694.3 $[\text{M} - \text{PF}_6]^+$. HRMS (ESI+) m/z for $\text{C}_{39}\text{H}_{26}\text{N}_7\text{Ru}$: calcd 694.1288, found 694.1274. HPLC retention time: 29.20 min.

[Ru(bpy)₂(pbpn)]PF₆ (4). [Ru(bpy)₂(pbpn)]PF₆ was synthesized using an adapted literature procedure.⁴⁷ Ru(bpy)₂Cl₂·2H₂O (150 mg, 0.29 mmol) and pbpn (68 mg, 0.21 mmol) were added to a microwave vessel containing a mixture of triethylamine (1 mL) and ethylene glycol (3 mL). The solution was subjected to microwave irradiation at 120 °C for 1 h and then pipetted into 30 mL of a stirring saturated KPF₆ solution. The resulting precipitate was collected under vacuum on a fine glass-sintered frit and purified by silica gel column chromatography with 5% MeOH in DCM. Purple solid (42 mg, 23%). $R_f = 0.76$ (10% H₂O + 2.5% sat. KNO₃ in MeCN). ^1H NMR (500 MHz, MeCN-*d*₃): δ 9.30 (dd, $J = 8.0$, 1.4 Hz, 1H, c), 8.94 (d, $J = 5.5$ Hz, 2H, g, l), 8.60 (dd, $J = 7.8$, 1.1 Hz, 1H, f), 8.51 (d, $J = 8.3$, 1H, 3A), 8.42–8.37 (m, 2H, 3B, 3C), 8.34 (d, $J = 8.2$ Hz, 1H, 3D), 8.30–8.25 (m, 2H, h, k), 8.13–8.07 (m, 1H, 6C), 8.05 (td, $J = 7.9$, 1.6 Hz, 1H, 4A), 8.00–7.94 (m, 2H, 6A, a), 7.92–7.85 (m, 3H, 4B, 6B, 6D), 7.81–7.76 (m, 2H, 4C, 4D), 7.70–7.63 (m, 2H, i, j), 7.48 (ddd, $J = 7.7$, 5.3, 1.2 Hz, 1H, 5A), 7.40 (dd, $J = 8.0$, 5.4 Hz, 1H, b), 7.33 (t, $J = 7.5$ Hz, 1H, e), 7.30 (ddd, $J = 7.4$, 5.7, 1.4 Hz, 1H, 5B), 7.15–7.10 (m, 2H, 5C, 5D), 6.88 (dd, $J = 7.2$, 1.1 Hz, 1H, d). ^{13}C NMR (75 MHz, MeCN-*d*₃): δ 188.19, 157.95, 154.73, 154.62, 153.96, 153.63, 152.28, 151.27, 149.13, 147.40, 147.07, 146.15, 141.66, 139.50, 139.40, 135.86, 135.62, 135.01, 134.20, 133.34, 131.97, 131.20, 130.92, 130.81, 130.69, 128.67, 128.38, 125.71, 125.57, 125.11, 124.38, 124.14, 124.00, 123.78, 123.77, 123.57, 123.11, 123.03, 122.81, 120.22, 120.03, 119.78, 119.39. MS (ESI+) m/z 744.4 $[\text{M} - \text{PF}_6]^+$. HRMS ESI+ m/z for $\text{C}_{43}\text{H}_{28}\text{N}_7\text{Ru}$: calcd 744.1444, found 744.1450. HPLC retention time: 30.92 min.

2.4. Spectroscopy. Photophysical characterization was carried out on dilute solutions (5 μM) of the PF₆[−] salts of the metal complexes in spectroscopic-grade MeCN unless otherwise noted. Molar extinction coefficients at wavelength maxima were determined from the slopes ϵ of linear fits of absorption versus concentration plots ($A = \epsilon bc$). Five concentrations (20 μM and four serial dilutions of 25%) were used with points measured in duplicate. Quantum yields for emission (Φ_{em}) and singlet oxygen (Φ_{Δ}) were measured relative to [Ru(bpy)₃](PF₆)₂ according to eq 1, where I , A , and η are integrated emission intensity, absorbance at the excitation wavelength, and refractive index of the solvent, respectively. Reference values used for [Ru(bpy)₃](PF₆)₂ as the standard are as follows: $\Phi_{\text{em}} = 0.012$ at 298 K in aerated MeCN,⁴⁸ $\Phi_{\text{em}} = 0.062$ at 298 K in deaerated MeCN, $\Phi_{\text{em}} = 0.38$ at 77 K in frozen 4:1 v/v EtOH:MeOH,¹⁰ and $\Phi_{\Delta} = 0.56$ in aerated MeCN.⁴⁹

$$\Phi_{\text{em}} = \Phi_{\text{s}} \left(\frac{I}{A} \right) \left(\frac{A_{\text{s}}}{I_{\text{s}}} \right) \left(\frac{\eta^2}{\eta_{\text{s}}^2} \right) \quad (1)$$

Where relevant, oxygen was removed from room temperature samples in long-neck cuvettes (Luzchem SC-10L) by purging with argon at a pressure of 50 ± 10 mmHg for 30 min. Samples for 77 K measurements were prepared in 4:1 EtOH:MeOH in a 5 mm i.d. NMR tube that was placed in a quartz-tipped cold finger Dewar (fabricated by Wilmad Labglass) filled with liquid nitrogen. Absorption spectra were recorded with a Jasco V-530 spectrophotometer. Steady-state luminescence spectra were measured on a PTI Quantamaster equipped with a K170B PMT for measuring ultraviolet to visible emission and a Hamamatsu R5509-42 near-IR PMT for measuring near-infrared (near-IR) emission (<1400 nm). Phosphorescence lifetimes (<1 μs) were measured on a PTI LaserStrobe spectro-

fluorometer with an R928 stroboscopic detector with excitation from a GL-3300 nitrogen/GL-301 dye laser (2–3 nm fwhm). Excited-state lifetimes were extracted from the observed data using PTI Felix32 fitting software. Emission and excitation spectra were corrected for the wavelength dependence of lamp output and detector response.

2.5. Cellular Assays. **2.5.1. Metal Compound Solutions.** Stock solutions of the chloride salts of the Ru(II) complexes were prepared at 5 mM in 10% DMSO in water and kept at -20 °C prior to use. Working dilutions were made by diluting the aqueous stock with pH 7.4 Dulbecco's phosphate buffered saline (DPBS). DPBS is a balanced salt solution of 1.47 mM potassium phosphate monobasic, 8.10 mM sodium phosphate dibasic, 2.68 mM potassium chloride, and 0.137 M sodium chloride (no Ca^{2+} or Mg^{2+}). DMSO in the assay wells was under 0.1% at the highest complex concentration.

2.5.2. Cell Culture. **HL-60.** HL-60 human promyelocytic leukemia cells (ATCC CCL-240) were cultured at 37 °C under 5% CO₂ in RPMI 1640 (Mediatech Media MT-10-040-CV) supplemented with 20% FBS (PAA Laboratories, A15-701) and were passaged 3–4 times per week according to standard aseptic procedures. Cultures were started at 200,000 cells mL^{−1} in 25 cm² tissue culture flasks and were subcultured when growth reached 800,000 cells mL^{−1} to avoid senescence associated with prolonged high cell density. Complete growth medium was prepared in 200 mL portions as needed by combining RPMI 1640 (160 mL) and FBS (40 mL, prealiquoted and heat inactivated) in a 250 mL Millipore vacuum stericup (0.22 μm) and filtering.

SK-MEL-28. Adherent SK-MEL-28 malignant melanoma cells (ATCC HTB-72) were cultured in Eagle's Minimum Essential Medium (EMEM, Mediatech Media MT-10-009-CV) supplemented with 10% FBS, were incubated at 37 °C under 5% CO₂, and were passaged 2–3 times per week according to standard aseptic procedures. SK-MEL-28 cells were started at 200,000 cells mL^{−1} in 75 cm² tissue culture flasks and were subcultured when growth reached 550,000 cells mL^{−1} by removing old culture medium and rinsing the cell layer once with Dulbecco's phosphate buffered saline (DPBS 1 \times , Mediatech, 21-031-CV), followed by dissociation of the cell monolayer with trypsin-EDTA solution (0.25% w/v Trypsin/0.53 mM EDTA, ATCC 30-2101). Complete growth medium was added to the cell suspension to allow appropriate aliquots of cells to be transferred to new cell vessels. Complete growth medium was prepared in 150 mL portions as needed by combining EMEM (135 mL) and FBS (15 mL, prealiquoted and heat inactivated) in a 250 mL Millipore vacuum stericup (0.22 μm) and filtering.

2.5.3. Cytotoxicity and Photocytotoxicity. Cell viability experiments were performed in triplicate in 96-well ultra-low attachment flat bottom microtiter plates (Corning Costar, Acton, MA), where outer wells along the periphery contained 200 μL of DPBS (2.68 mM potassium chloride, 1.47 mM potassium phosphate monobasic, 0.137 M sodium chloride, and 8.10 mM sodium phosphate dibasic) to minimize evaporation from sample wells. Cells growing in log phase (HL-60 cells: \sim 800,000 cells mL^{−1}. SK-MEL-28 cells: \sim 550,000 cells mL^{−1}) with at least 93% viability were transferred in 50 μL aliquots to inner wells containing warm culture medium (25 μL) and placed in a 37 °C, 5% CO₂ water-jacketed incubator (Thermo Electron Corp., FormaSeries II, Model 3110, HEPA Class 100) for 3 h to equilibrate (and allow for efficient cell attachment in the case of SK-MEL-28 adherent cells). Metals compounds were serially diluted with DPBS and prewarmed at 37 °C before 25 μL aliquots of the appropriate dilutions were added to cells. PS-treated microplates were incubated at 37 °C under 5% CO₂ for 16 h drug-to-light intervals. Control microplates not receiving a light treatment were kept in the dark in an incubator, and light-treated microplates were irradiated under one of the following conditions: visible light (400–700 nm, 34.2 mW cm^{−2}) using a 190 W BenQ MS 510 overhead projector or red light (625 nm, 29.1 mW cm^{−2}) from an LED array (PhotoDynamic Inc., Halifax, NS). Irradiation times using these two light sources were approximately 49 and 57 min, respectively, to yield total light doses of 100 J cm^{−2}. Both untreated and light-treated microplates were incubated for another 48 h before 10 μL aliquots of prewarmed Alamar Blue reagent (Life Technologies DAL 1025) were added to all sample wells and

subsequently incubated for another 15–16 h. Cell viability was determined on the basis of the ability of the Alamar Blue redox indicator to be metabolically converted to a fluorescent dye by only live cells. Fluorescence was quantified with a Cytofluor 4000 fluorescence microplate reader with the excitation filter set at 530 ± 25 nm and emission filter set at 620 ± 40 nm. EC_{50} values for cytotoxicity (dark) and photocytotoxicity (light) were calculated from sigmoidal fits of the dose–response curves using Graph Pad Prism 6.0 according to eq 2, where y_i and y_f are the initial and final fluorescence signal intensities. For cells growing in log phase and of the same passage number, EC_{50} values are generally reproducible to within $\pm 25\%$ in the submicromolar regime, $\pm 10\%$ below $10 \mu\text{M}$, and $\pm 5\%$ above $10 \mu\text{M}$. Phototherapeutic indices (PIs), a measure of the therapeutic window, were calculated from the ratio of dark to light EC_{50} values obtained from the dose–response curves.

$$y = y_i + \frac{y_f - y_i}{1 + 10^{(\log EC_{50} - x) \times (\text{Hillslope})}} \quad (2)$$

2.6. DNA Photocleavage Assays. DNA photocleavage experiments were performed according to a general plasmid DNA gel mobility shift assay^{16,50,51} with $30 \mu\text{L}$ total sample volumes in 0.5 mL microfuge tubes. Transformed pUC19 plasmid ($3 \mu\text{L}$, $>95\%$ form I) was added to $15 \mu\text{L}$ of 5 mM Tris-HCl buffer supplemented with 50 mM NaCl (pH 7.5). Serial dilutions of the Ru(II) compounds were prepared in ddH₂O and added in $7.5 \mu\text{L}$ aliquots to the appropriate tubes to yield final Ru(II) concentrations ranging from 1 to $100 \mu\text{M}$. Then, ddH₂O ($4.5 \mu\text{L}$) was added to bring the final assay volumes to $30 \mu\text{L}$. Control samples with no metal complex received $12 \mu\text{L}$ of water. Sample tubes were kept at $37 \text{ }^\circ\text{C}$ in the dark or irradiated. Light treatments employed visible light (14 J cm^{-2}) delivered from a Luzchem LZC-4X photoreactor over the course of 30 min . After treatment, all samples (dark and light) were quenched by the addition of $6 \mu\text{L}$ of gel loading buffer (0.025% bromophenol blue, 40% glycerol). Samples ($11.8 \mu\text{L}$) were loaded onto 1% agarose gels cast with $1 \times$ TAE (40 mM Tris-acetate, 1 mM EDTA, pH 8.2) containing ethidium bromide ($0.75 \mu\text{g mL}^{-1}$) and electrophoresed for 30 min at 80 V cm^{-1} in $1 \times$ TAE. The bands were visualized using the Gel Doc-It Imaging system (UVP) with Vision Works software and further processed with the GNU Image Manipulation Program (GIMP).

2.7. Confocal Microscopy. Sterile glass-bottom Petri dishes (MatTek) were coated with $200 \mu\text{L}$ poly-L-lysine (Ted Pella) in a laminar flow hood under standard aseptic conditions. After a 1 h incubation period at $37 \text{ }^\circ\text{C}$, 5% CO₂ in a water-jacketed incubator (Thermo Electron Corp., Forma Series II, Model 3110, HEPA class 100), the dishes were washed three times with sterile Dulbecco's phosphate buffered saline (DPBS $1 \times$, Mediatech, 21-031-CV) containing 2.68 mM potassium chloride, 1.47 mM potassium phosphate monobasic, 0.137 M sodium chloride, and 8.10 mM sodium phosphate dibasic, pH 7.4, and were left to dry uncovered at room temperature for approximately 15 min . HL-60 human promyelocytic leukemia cells (ATCC CCL-240) or SK-MEL-28 malignant melanoma cells (ATCC HTB-72) were then transferred in aliquots of $500 \mu\text{L}$ (approximately $100,000$ cells) to the poly-L-lysine-coated glass bottom Petri dishes and were allowed to adhere for 15 min or 2 h , respectively, in a $37 \text{ }^\circ\text{C}$, 5% CO₂ water-jacketed incubator. Metal compound ($500 \mu\text{L}$ of a $10 \mu\text{M}$ solution in sterile PBS prewarmed to $37 \text{ }^\circ\text{C}$) was added to sample dishes (destined to receive either a dark or light treatment), which were returned to the incubator for 30 min prior to further treatment; control dishes that did not contain the metal compound were also prepared. Light-treated samples were irradiated with visible light for 24 min from a 190 W BenQ MS 510 overhead projector ($400\text{--}700 \text{ nm}$, power density = 34.2 mW cm^{-2} , total light dose $\approx 50 \text{ J cm}^{-2}$) or with red light for 28 min from an LED array (625 nm , power density = 29.1 mW cm^{-2} , total light dose $\approx 50 \text{ J cm}^{-2}$). Dark samples were covered with foil and placed in a drawer for the same amount of time. Cells were then imaged at 15 min post-treatment using a Carl Zeiss LSM 510 laser scanning confocal microscope with a $40 \times$ oil objective lens. Excitation was delivered at $458/488 \text{ nm}$ from an argon–krypton laser, and signals were acquired through a 475 nm long-pass filter. Pinhole diameters for

all the treatments were $200 \mu\text{m}$. The images were collected and analyzed using the Zeiss LSM Image Browser Version 4.2.0.121 software (Carl Zeiss Inc.).

Intracellular production of reactive oxygen species (ROS) was detected in HL-60 cells and SK-MEL-28 cells using the ROS fluorescent dye dihydroethidium (DHE) (VWR, 38483-26-0) according to the manufacturer's protocol. Cells loaded with the metal compound were then washed with DPBS and incubated with $3 \mu\text{M}$ DHE at $37 \text{ }^\circ\text{C}$ for 15 min before receiving a dark or light (visible or red, 50 J cm^{-2}) treatment. Visible and red light treatments were delivered from the sources described in section 2.5.3. Production of ROS was imaged using a Carl Zeiss LSM 510 laser scanning confocal microscope with a $40 \times$ oil objective lens. Excitation was delivered at $458/488 \text{ nm}$ from an argon–krypton laser, and signals were acquired through a 510 nm long-pass filter and a $475\text{--}525 \text{ nm}$ band-pass filter. The pinhole diameter for all of the treatments was $200 \mu\text{m}$. The images were collected and analyzed using Zeiss LSM Image Browser Version 4.2.0.121 software (Carl Zeiss Inc.).

3. RESULTS AND DISCUSSION

3.1. Synthesis and Characterization. Following the seminal discovery that electron-withdrawing groups added to cyclometalating ligands of the type p^-ppy^- could position the Ru^{III/II} couple at the same energy as that of the champion N3 photosensitizer,³⁵ a growing number of functionalized cyclometalated ligands are now being explored for dye-sensitized solar cells.^{1,52} Functionalization of p^-ppy^- has generally involved only mono- or disubstitution with electron-withdrawing atoms, groups, or rings rather than fused π -systems. Even bhq^- as an alternate cyclometalating ligand remains relatively underutilized owing to the ease with which p^-ppy^- can be substituted and subsequently coordinated to Ru(II). Thus, incorporation of extended π -systems directly into cyclometalating bidentate frameworks has not been explored.

Therefore, we chose to investigate the novel cyclometalating analogue of the benzo[*i*]dipyrido[3,2-*a*:2',3'-*c*]phenazine (dppn) ligand, pbpn, out of our interest in π -expansive ligands that contribute low-lying triplet intraligand (IL) excited states that are highly photosensitizing.¹⁵ To probe the effects of π -conjugation on the photophysics and photobiological activities of the cyclometalated systems (and to compare with their Ru(II) polypyridyl counterparts), we also prepared pbpz and pbpq. These three new ligands were synthesized from benzo[*h*]quinoline-5,6-dione via a condensation reaction with the corresponding diamines in alcoholic solvent at reflux. Yields ranged from 30% for pbpq to 67% for pbpn and increased with the number of fused rings. The starting benzo[*h*]quinoline-5,6-dione was obtained in almost quantitative yield by oxidation of commercial bhq with iodopentoxide in glacial acetic acid.^{44,53} ¹H NMR and two-dimensional ¹H–¹H COSY NMR spectroscopy were used to characterize these new ligands as well as bhq and benzo[*h*]quinoline-5,6-dione. The chemical shifts for bhq were reported previously with hydrogens *f*–*h* assigned incorrectly using 1D NMR.⁵⁴ With 2D techniques, we have corrected these assignments (Figure S1).

A recent method for generating a variety of cycloruthenated compounds involves the preparation of a Ru π -arene, dimeric [$\pi\text{-C}_6\text{H}_6\text{RuCl}_2$]₂ in the solid state,⁵⁵ from 1,3-cyclohexadiene and RuCl₃·*x*H₂O, and its subsequent reaction with the cyclometalating ligand in MeCN to produce the corresponding [Ru(CH₃CN)₄(C^N)]PF₆ complex.^{34,56} This air-sensitive intermediate,⁵⁷ which is then reacted with the desired coligands, normally requires purification and is only stable under ambient conditions for a few hours. Older methods that

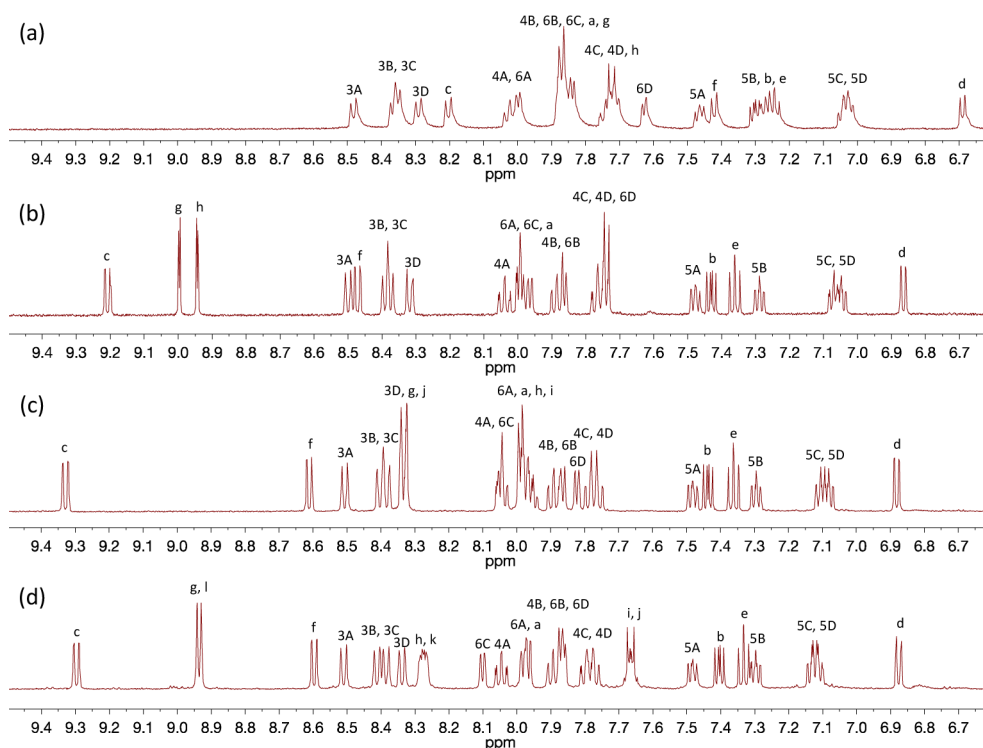


Figure 1. ^1H NMR spectra collected for compounds **1** (a), **2** (b), **3** (c), and **4** (d) in d_3 -MeCN.

employ the more stable *cis*-Ru(bpy) $_2$ Cl $_2$ require long reaction times at reflux and the use of silver(I) salts to abstract chloride ions.⁵⁸ We sought an alternate method for preparing bis-heteroleptic Ru(II) C $^{\wedge}$ N systems that could be carried out in air without Ag(I) ions using microwave irradiation to ensure short reaction times while avoiding oxygen-sensitive intermediates. Use of 1:3 NEt $_3$:ethylene glycol⁴⁷ for reacting *cis*-Ru(LL) $_2$ Cl $_2$ (LL = bpy or some other diimine ligand) with a wide range of cyclometalating ligands led to identifiable product by TLC in 1 h or less at 120 $^{\circ}\text{C}$ with unoptimized yields of approximately 25%. These yields are as good or better than those previously reported with more cumbersome steps. Compounds **1**–**4** were synthesized using this methodology, and their structures were confirmed by 1D ^1H NMR and 2D ^1H – ^1H COSY NMR as well as HPLC and mass spectrometry.

Two-dimensional ^1H – ^1H COSY NMR has previously been used to assign all 20+ protons of certain cyclometalated [Ru(bpy) $_2$ (phpy $^-$)] $^+$ derivatives.^{31,59,60} The low microsymmetry of the overall pseudo octahedral complex imparted by the asymmetric cyclometalating ligand translates to nonequivalence of all 16 bpy protons alongside those of the C $^{\wedge}$ N ligand. Therefore, a complex such as **4** would be expected to yield 28 unique signals (26 for **3**, 24 for **2**, and 24 for **1**). To our knowledge, the proton spectrum of previously reported **1** has not been assigned.⁶¹ A close analysis of the similarities and differences in the 1D and 2D ^1H NMR spectra obtained for compounds of the present series scrutinized alongside the published [Ru(bpy) $_2$ (phpy $^-$)] $^+$ assignments afforded the opportunity to decipher otherwise rather complex spectra characterized by overlapping multiplets.

X-ray crystallographic evidence³¹ of shortened Ru–C bond distances that lead to elongated Ru–N bonds *trans* and *cis* relative to the Ru–C coordination axis, with the *trans* effect being greater, provided the basis for our interpretation and assignments (Figures S6–7, S9, and S11). Qualitatively, these

distortions bring ring F and its hydrogens closer to the metal center while pushing rings A, B, and E and their respective hydrogens farther from Ru(II) (Chart 1). The impact was greatest for hydrogen *d* next to the Ru–C bond, which was the most shielded proton in all of the complexes investigated, and for hydrogen *c* in **2**–**4**, which was the most deshielded proton.

Hydrogen *d*, adjacent to the chelating carbon of the C $^{\wedge}$ N ligand and shielded due to the shortened Ru–C bond distance of ring F, was diagnostic for all of the complexes, giving rise to a doublet at substantially lower frequencies (6.7–6.9 ppm) than the other aromatic proton signals (Figure 1). The other diagnostic peak for complexes **2**–**4** was produced by proton *c* and occurred as a doublet at substantially higher frequencies (9.15–9.35 ppm) than the rest of the aromatic signals owing to the lengthening of the Ru–N bond of ring E combined with its proximity to the nitrogen of the electron-deficient pyrazine ring. When pyrazine was absent, as for compound **1**, the signal for proton *c* occurred upfield at 8.2 ppm, and no signals were shifted higher than 8.5 ppm. This proximity effect was further supported by the appearance of deshielded signals corresponding to protons *g* and *h* near 9.0 ppm for **2**, and *g* and *l* near 8.9 ppm for **4**. Interestingly, the signals for protons *g* and *l* of **4**, which correspond to protons *g* and *l* of **3**, occurred at much lower frequencies (8.3–8.4 ppm), underscoring the influence of increased π -conjugation and the necessity for detailed 2D NMR analysis for each new complex. All other protons of the C $^{\wedge}$ N ligands were assigned based on their coupling profiles in the ^1H – ^1H COSY spectra obtained for the complexes and their corresponding ligands and by comparing these profiles between different ligands and complexes within the series (Figures S1–7, S9, and S11).

The resonant frequencies for all 16 nonequivalent bpy protons of **1**–**4** (Chart 1) were assigned based on established trends for *cis*-[Ru(bpy) $_2$ LL] $^{2+}$ complexes (whereby, in general, H3 > H4 > H6 > H5),^{41,59} the bond distances reported by

Sasaki et al.⁶⁰ for cyclometalated phpy^- complexes, $^1\text{H}-^1\text{H}$ correlations, and coupling constants. The chemical shifts of the bpy proton signals increased by ring in the order $A > B > C > D$. The ring protons of A and B were the most deshielded of the bpy protons due to the longer Ru–N bond distance reported for ring A (and to a lesser extent ring B), whereas the protons of ring D were shielded the most due to their close proximity to C \wedge N ring E. Within any one bpy ring, the chemical shifts followed $\text{H3} > \text{H4} > \text{H6} > \text{H5}$ with a few exceptions: 1, ring C, $6 > 4$; 2, ring C, $6 > 4$; 3, rings C and D, $6 > 4$; and 4, rings C and D, $6 > 4$.

3.2. Photophysical Properties. **3.2.1. Absorption.** Electronic absorption spectra for complexes 1–4 were collected in MeCN at room temperature (Figure 2). The spectroscopic

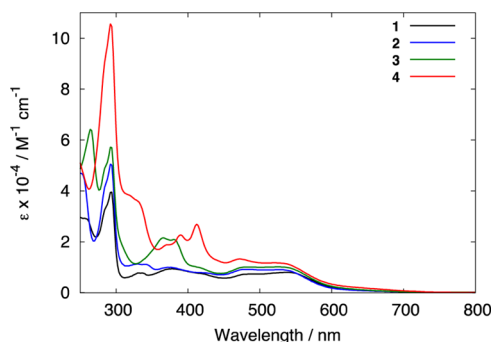


Figure 2. Ground-state absorption spectra of 1–4 in MeCN at room temperature.

signature of 1 has been reported,³³ with the sharp bands in the 250–300 nm region assigned to $\pi\pi^*$ transitions involving the bpy and bhq^- ligands, and the two sets of low-energy bands between 320 and 700 nm assigned to MLCT transitions. The previous report designated the lower energy MLCT band (450–800 nm) as possessing $\text{Ru}^{2+} \rightarrow \text{bpy}$ parentage and the higher energy band (345–450 nm) of $\text{Ru}^{2+} \rightarrow \text{C}\wedge\text{N}$ parentage. Numerous spectroscopic and electrochemical techniques employed in that study confirmed that the lowest energy charge-transfer excited state for 1 retains pure $\text{Ru}^{2+} \rightarrow \text{bpy}$ character and that the C \wedge N unit serves as an ancillary ligand. CT transitions were characterized by maximum extinction coefficients near $10,000 \text{ M}^{-1} \text{ cm}^{-1}$, but we observed slightly smaller ϵ values ($7,400\text{--}9,400 \text{ M}^{-1} \text{ cm}^{-1}$) for 1.

Fusing a pyrazine ring to the cyclometalating bhq^- to form the more π -expansive pbpq ligand (complex 2) gave rise to a qualitatively similar absorption profile with the $\text{Ru}^{2+} \rightarrow \text{bpy}$ transitions occurring at slightly shorter wavelengths and ϵ being marginally larger throughout the spectrum. However, the introduction of additional fused benzene rings beyond pyrazine produced substantial changes in the absorption spectra, as exemplified for compounds 3 and 4. Extinction coefficients for 3 and 4 were larger at all wavelengths, and notably, new bands formed between 300 and 450 nm that overlapped the $\text{Ru}^{2+} \rightarrow \text{C}\wedge\text{N}$ MLCT transitions. These new features were attributed to longer wavelength $\pi\pi^*$ transitions (with possible contribution from $n\pi^*$ transitions) centered on the more π -expansive cyclometalating ligands. A comparison shown for compound 4 and its corresponding C \wedge N ligand (pbpn) supports this interpretation (Figure 3). Although the absorption spectra for the complex and its C \wedge N ligand were collected in different solvents (owing to solubility differences), the characteristic pattern produced by pbpn was clearly observable in the

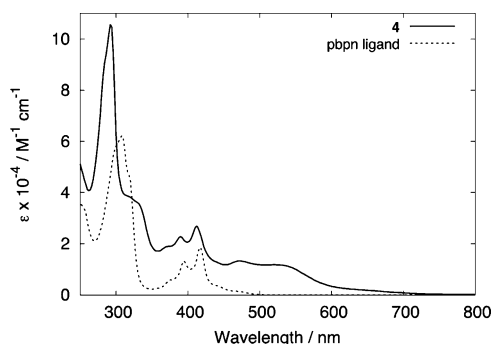


Figure 3. Ground-state absorption spectrum of 4 in MeCN compared to that of its free cyclometalating ligand in CHCl_3 at room temperature.

spectrum of 4 with only slight differences in the peak maxima of the fingerprint vibronic progression.

3.2.2. Emission. Static and dynamic photoluminescence measurements were made for compounds 1–4 at room temperature (argon-saturated MeCN) and at 77 K (4:1 EtOH:MeOH glass). Compounds 1–3 produced very weak broad, structureless phosphorescence in solution at room temperature ($\Phi_{\text{em}} \sim 10^{-4}$) centered near 800 nm (Table 1), and 4 displayed no discernible $^3\text{MLCT}$ emission in this region. The excitation spectra for MLCT emission from 1–3 superimposed the corresponding absorption profiles in the MLCT regions. Quantum efficiencies for MLCT emission are listed in Table 1, but their yields were too small to make reliable quantitative comparisons. As expected, emission lifetimes measured near 800 nm at 298 K for 1–3 were extremely short (5–20 ns) compared to related Ru(II) polypyridyl complexes ($\sim 1 \mu\text{s}$)¹⁰ and agreed with the reported lifetime for 1 (20 ns). For example, in deoxygenated MeCN, the $^3\text{MLCT}$ lifetime of the prototype $[\text{Ru}(\text{bpy})_3]^{2+}$ is as long as $1 \mu\text{s}$ in fluid solution at room temperature,¹⁰ whereas that of the analogous $[\text{Ru}(\text{bpy})_2\text{phpy}]^+$ complex is almost 2 orders of magnitude shorter.³³ Radiative and nonradiative decay rate constants were not calculated for the present series owing to the error associated with Φ_{em} values < 0.005 .

Relative to room temperature emission, the phosphorescence from 1–3 at low temperature (77 K in 4:1 EtOH:MeOH glass) shifted to higher energies, increased in intensity, and displayed characteristic $^3\text{MLCT}$ vibronic structure (Figure 4). Quantum yields and lifetimes increased up to 127- and 89-fold, respectively, at low temperature but were still substantially reduced relative to their Ru(II) diimine counterparts according to the energy gap law. The vibronic intervals were $1140\text{--}1220 \text{ cm}^{-1}$, which is diagnostic of diimine involvement in the emissive excited state.⁶² Together, these factors support the notion that the lowest energy MLCT states are of $\text{Ru}^{2+} \rightarrow \text{bpy}$ origin. Further, the thermally induced Stokes shifts (ΔE_s) for complexes 1–3 ranged from 1230 cm^{-1} for 1 to 1435 cm^{-1} for 2, which is consistent with ΔE_s for $[\text{Ru}(\text{bpy})_3]^{2+}$ under identical conditions (1127 cm^{-1}). This relatively large value for ΔE_s is in agreement with what is expected from polar excited states of $^3\text{MLCT}$ character.⁶³ The onset of the structured emission from 2 and 3 was blue-shifted by approximately 248 cm^{-1} relative to 1, suggesting that the pyrazine ring may facilitate delocalization of the HOMO orbital onto the cyclometalating ligand, reducing structural distortion between the ground and emissive excited state.³⁵

Table 1. Photophysical Properties of 1–4

compound	λ_{abs} [nm] (log ϵ)	λ_{em} [nm] ^{a,b}		$\Phi_{\text{em}} (\times 10^{-4})$ ^{a,b}		τ [ns] ^{a,b}		$\Phi_{\Delta} (\times 10^{-2})$ ^{a,c}
		298 K	77 K	298 K	77 K	298 K	77 K	
1	542 (3.90), 486 (3.87), 382 (3.97), 332 (3.89), 294 (4.60)	802	730	2.3	91	20	388	6.8
2	532 (3.95), 480 (3.96), 376 (4.00), 294 (4.70), 250 (4.67)	798	716	5.8	100	20	498	7.6
3	528 (4.01), 482 (4.00), 382 (4.32), 366 (4.33), 294 (4.76)	800	718	1.1	140	6.6	588	1.3
4	532 (4.06), 476 (4.12), 414 (4.42), 392 (4.35), 294 (5.02)		718, 800		110		527, 404	0.56

^aMeasured with excitation at the longest-wavelength absorption maximum corresponding to the $\text{Ru}^{2+} \rightarrow \text{bpy}$ transition. ^bMeasurements at 298 K were performed on argon-purged samples in MeCN; 77 K measurements were performed in air-saturated EtOH:MeOH (4:1) glasses. ^cAir-saturated MeCN at 298 K assuming 21% O_2 .

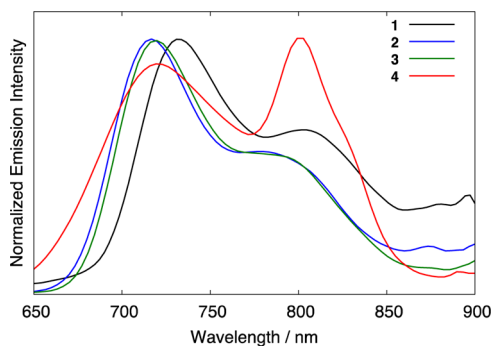


Figure 4. Normalized low-temperature emission spectra of 1–4 in 4:1 EtOH:MeOH glass at 77 K with $\lambda_{\text{ex}} = 542$ (1), 532 (2), 528 (3), and 532 (4) nm.

Although not emissive at room temperature, compound 4 displayed structured phosphorescence at 77 K with an onset similar to 2 and 3 at 718 nm (Figure 4). The largest peak in the vibronic progression of 4, however, was the sharp transition centered at 800 nm (overlapping what looks to be the expected ν_{0-1} band), making the 77 K spectrum for 4 quite distinct from the rest of the series. Nevertheless, its low-temperature Φ_{em} of 0.011% and lifetime of 527 ns were similar to other members of the series with $\text{Ru}^{2+} \rightarrow \text{bpy}$ emissive character. ΔE_s could not be determined for complex 4 because it produced no measurable $^3\text{MLCT}$ emission at room temperature. It is tempting to speculate that the low-energy phosphorescence from 4 at 77 K may have contributions from both $\text{Ru}^{2+} \rightarrow \text{bpy}$ and $\text{Ru}^{2+} \rightarrow \text{C}^{\wedge}\text{N}$ states. In fact, the lifetime measured at 800 nm was 100 ns shorter than that measured at 718 nm, and the two emission wavelengths gave rise to excitation spectra with some differences as well. If this is the case, then π -expansion on the cyclometalating ligand should have the ability to significantly impact the ensuing photophysical dynamics given the mixed orbital parentage of the excited state(s) that presumably dominates the trajectory. The observation that similar scaffolds in tridentate cyclometalated Ru(II) systems can lengthen excited state lifetimes by more than 5 orders of magnitude relative to $[\text{Ru}(\text{tpy})_2]^{2+}$ ($\tau = 120$ ps) attests to the profound influence that π -expansive ligands can have on photophysical dynamics.⁴⁶

Interestingly, the π -extended cyclometalated complexes exhibited ligand-centered (LC) fluorescence at room temperature; this phenomenon was not observed for 1. Although 528 nm excitation of 4 produced no $^3\text{MLCT}$ emission at room temperature, singlet emission from an LC state was readily apparent at 562 nm (Figure 5) and was greatest with $\lambda_{\text{ex}} = 312$ nm. The assignment was made based on the similarity of the LC emission from 4 to the free pbpn ligand measured in CHCl_3

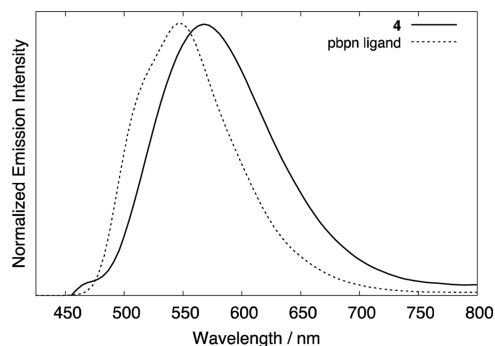


Figure 5. Normalized room-temperature emission spectra of 4 and its free cyclometalating ligand pbpn in MeCN and CHCl_3 , respectively.

($\lambda_{\text{em max}} = 548$ nm); complexation to Ru(II) broadened this emission slightly with a concomitant bathochromic shift of 14 nm. Free and complexed LC lifetimes were too short to quantify reliably in our experiments (<10 ns), which also supports the assignment as a singlet emission. Similar LC emission occurred at 375 ($\lambda_{\text{ex max}} = 290$ nm) and 523 nm ($\lambda_{\text{ex max}} = 294$ nm) for compounds 2 and 3, respectively. Green fluorescence from π -expansive cyclometalated complexes such as 4 could be exploited for diagnostic purposes in photobiological applications.

3.2.3. Singlet Oxygen Sensitization. Quantum yields for singlet oxygen production (Φ_{Δ}) by 1–4 were measured in air-saturated MeCN solution and calculated from sensitized $^1\text{O}_2$ emission (centered at 1268 nm) relative to $[\text{Ru}(\text{bpy})_3]^{2+}$ as the standard, which has been reported as 56% in aerated MeCN.⁴⁹ The cyclometalated compounds were poor $^1\text{O}_2$ generators with Φ_{Δ} values generally less than 8% (Table 1). Compounds 1 and 2 gave the largest yields in the range of 7–8%, 3 was near 1%, and 4 was less than 1%. These values did not change appreciably when measured in water. By comparison, the related Ru(II) polypyridyl complexes, such as 5, 6 and 8, typically yield $^1\text{O}_2$ with 80–90% quantum efficiencies^{15,64,65} with $[\text{Ru}(\text{bpy})_2\text{dppz}]^{2+}$ (7) known to be lower at 15–20%.⁶⁴ It is not surprising that the cyclometalated Ru(II) compounds yield less singlet oxygen given that their excited state decay is heavily influenced by the energy gap law. Presumably efficient $^3\text{MLCT} \rightarrow ^1\text{MLCT}$ nonradiative coupling afforded by low-energy $^3\text{MLCT}$ states competes effectively with other modes of excited state deactivation, namely, $^1\text{O}_2$ sensitization and phosphorescence.

3.3. Photobiological Activity. **3.3.1. Cytotoxicity and Photocytotoxicity.** Previous investigations involving cyclometalated Ru(II) complexes overwhelmingly indicate that in vitro cytotoxicity for this class is extremely high, categorizing these compounds more accurately as potential chemo-

Table 2. In Vitro Cytotoxicity and Photocytotoxicity Data for Cyclometalated Ru(II) Complexes 1–4 and Reference Ru(II) Polypyridyl Complexes 5–8 Obtained in Two Cell Lines

compd	EC ₅₀ (μM)					
	SK-MEL-28			HL60		
	dark	vis PDT ^a	PI ^b	dark	vis PDT ^a	PI ^b
1	1.94 ± 0.04	0.258 ± 0.009	7.5	1.29 ± 0.01	0.151 ± 0.001	8.6
2	1.16 ± 0.01	0.142 ± 0.002	8.3	3.06 ± 0.10	0.167 ± 0.003	18
3	1.92 ± 0.02	0.208 ± 0.003	9.1	1.14 ± 0.01	0.211 ± 0.004	5.4
4	>300	0.206 ± 0.003	>1,400	>300	0.741 ± 0.016	>410
5	>300	8.86 ± 0.12	>34	>300	19.52 ± 1.32	>15
6	>300	237 ± 7	>1.3	>300	253 ± 11	>1.2
7	>300	172 ± 5	>1.7	>300	166 ± 4	>1.8
8	265 ± 5	0.182 ± 0.005	1,500	282 ± 19	0.303 ± 0.020	>930

^aVis PDT: 16 h drug-to-light interval followed by 100 J cm⁻² visible-light irradiation. ^bPI = phototherapeutic index (ratio of dark EC₅₀ to light EC₅₀).

therapeutics rather than photodynamic or photoactivatable agents. For example, [Ru(bpy)(dppn)(phpy⁻)]⁺ gave an EC₅₀ value (concentration of compound required to kill 50% of a cell population) of 7 μM in HeLa cells in the dark,³⁶ and the very closely related compounds of the type [Ru(bpy)(phpy⁻)(LL)]⁺ (where LL = dpq or dppn) (dpq = dipyrido-3,2-*d*:2',3'-*f*]quinoxaline) were even more potent than cisplatin against all cancer cell lines screened (<10 μM).³⁸ For comparison, Ru(II) polypyridyl compounds of the type [Ru(bpy)₂LL]²⁺ (where LL = phen (5), dpq (6), dppz (7), or dppn (8)) (dppz = dipyrido[3,2-*a*:2',3'-*c*]phenazine) were essentially nontoxic in the dark (EC₅₀ > 100 μM) under comparable conditions in the two cell lines used in the present study (Table 2).

As might be expected, compounds 1–3, which are the cyclometalated counterparts to 5–7, were highly toxic to cancer cells in the dark. Their dark EC₅₀ values were 1–2 μM in SK-MEL-28 cells and 1–3 μM in HL-60 cells (Table 2), making 1–3 conventional anticancer agents. Notably, compound 4 was nontoxic to cells (dark EC₅₀ > 300 μM in both cell lines investigated) without light activation. In fact, 4 was less cytotoxic compared to its Ru(II) diimine counterpart 8 in both cell lines, which defies the conventional notion that the tris bidentate cyclometalated Ru(II) analogues are inherently more toxic. It is interesting to note the striking difference in dark cytotoxicity for compounds 3 and 4 (Figure 6), which differ by only one fused benzene ring. Compound 3 was >150 times more cytotoxic than 4 in SK-MEL-28 cells and almost 270

times more toxic in HL-60 cells. Therefore, π-expansion on at least one coordinating ligand of cyclometalating Ru(II) systems appears to be a requirement for suppressing dark cytotoxicity, but more importantly, the π-expansion must be on the C[^]N ligand in this limited series. The related [Ru(bpy)(phpy⁻)(dppn)]⁺ complex,³⁶ with the π-extended dppn and cyclometalating phpy⁻, is over 40× more toxic than compound 4. At present, it is not clear why [Ru(bpy)(phpy⁻)(dppn)]⁺ is substantially more cytotoxic. Differences in cellular uptake, localization, relocalization, efflux, and/or metabolism must play a role.

Photocytotoxicities of the cyclometalated Ru(II) compounds were submicromolar with a 100 J·cm⁻² visible light treatment. Light potencies varied from 142 nM (compound 2 in SK-MEL-28 cells) to 741 nM (compound 4 in HL-60 cells). Compounds 2 and 4 were slightly more phototoxic toward SK-MEL-28 cells, whereas 1 and 3 showed a slight phototoxic preference for HL-60 cells. Generally, the cytotoxicities of 1–3 were amplified less than 10-fold in the presence of a light trigger (compound 2 in HL-60 cells was an exception at almost 20-fold). These phototherapeutic indices (PIs), ratios of dark EC₅₀ values to light EC₅₀ values, were marginal compared to the light enhancements that were achieved for the more π-expansive 4.

Cyclometalated 4 was almost as potent toward SK-MEL-28 cells when compared to its diimine counterpart 8 (200 vs 180 nM) and was slightly less phototoxic toward HL-60 cells (740 vs 300 nM). Thus, π-expansion on the cyclometalating ligand can achieve similar light potencies as the π-expansive polypyridyl congeners that utilize highly photosensitizing, low-lying ³IL states (<2.1 eV). Given that the photocytotoxicities of Ru(II) polypyridyl complexes 5–7 (³IL energy > 2.1 eV) are significantly attenuated relative to 8 (and assuming that the ³IL energies of 5–7 are also >2.1 eV),⁶⁴ one can infer that the apparent photocytotoxicity observed for 1–3 is derived mainly from inherent dark cytotoxicity rather than contributing ³IL excited-state reactivity. Compounds 1–3 yielded low PIs in both cell lines, underscoring that the contribution of light-activation to photocytotoxicity is minimal for the less π-expansive systems. Compound 4, on the other hand, produced some of the largest PIs reported to date: >1,400 in SK-MEL-28 cells and >410 in HL-60 cells.^{11,25} It is clear that compound 4 is a highly effective light-responsive biological agent, and low-lying ³IL states combined with a low dark cytotoxicity may be key. As reported previously for 8 (and attributed to the presence of low-energy ³IL states),¹⁵ activation with monochromatic red light (625 nm) also produced photocytotoxicity

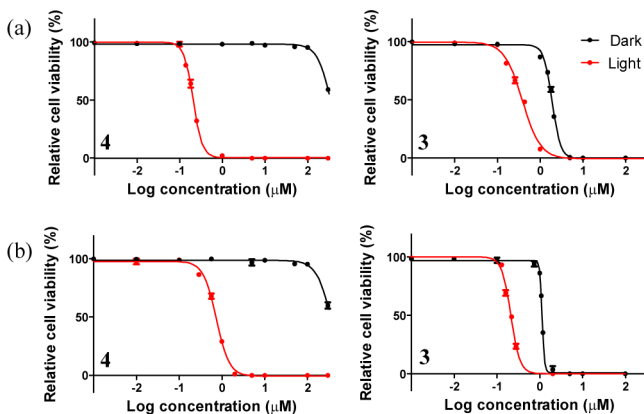


Figure 6. In vitro dose–response curves for compounds 3 (right panel) and 4 (left panel) in SK-MEL-28 (a) and HL-60 cells (b) with (red) and without (black) visible-light activation.

but with attenuated PIs relative to activation with broad-band visible light of the same dose.

3.3.2. Mechanistic Studies. DNA Interactions. An established cell-free DNA photocleavage assay^{16,50,51} was used to examine whether cyclometalated Ru(II) complexes could affect the structural integrity of DNA. Figure 7 outlines the dose–

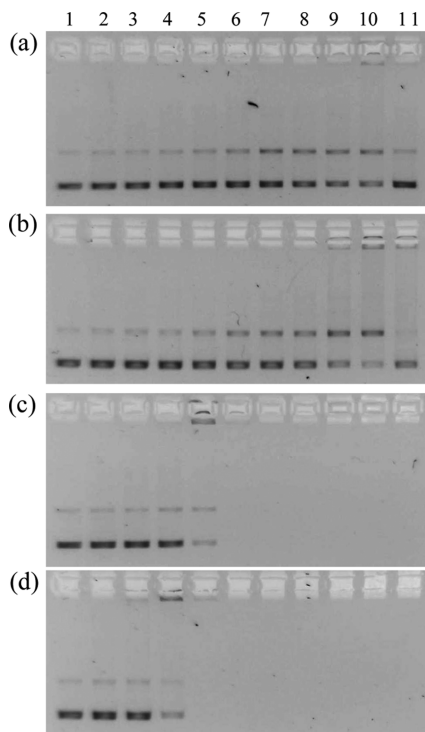


Figure 7. DNA photocleavage of pUC19 DNA (28.6 μM bases) dosed with metal complex (MC) **1** (a), **2** (b), **3** (c), or **4** (d) and visible light (14 J cm^{-2}). Gel mobility shift assays employed 1% agarose gels ($0.75 \mu\text{g mL}^{-1}$ ethidium bromide) electrophoresed in $1\times$ TAE at 8 V cm^{-1} for 30 min. Lane 1, DNA only ($-h\nu$); lane 2, DNA only ($+h\nu$); lane 3, $5 \mu\text{M}$ MC ($+h\nu$); lane 4, $20 \mu\text{M}$ MC ($+h\nu$); lane 5, $40 \mu\text{M}$ MC ($+h\nu$); lane 6, $60 \mu\text{M}$ MC ($+h\nu$); lane 7, $80 \mu\text{M}$ MC ($+h\nu$); lane 8, $100 \mu\text{M}$ MC ($+h\nu$); lane 9, $200 \mu\text{M}$ MC ($+h\nu$); lane 10, $300 \mu\text{M}$ MC ($+h\nu$); lane 11, $300 \mu\text{M}$ MC ($-h\nu$).

response profiles of **1–4** for damaging pUC19 plasmid DNA when activated with visible light. Lanes 1 and 2 are controls and demarcate mostly undamaged, supercoiled plasmid (form I). Lane 11 is also a control lane and represents the effect of the highest concentration of metal complex tested but without a light trigger. Two features were readily apparent. First, the cyclometalated compounds interfered with ethidium bromide staining in the order $4 > 3 > 1 \approx 2$, and for **3** and **4**, this interference occurred at high concentration even without a light treatment. Second, the Ru(II) cyclometalated compounds caused DNA aggregation/precipitation at the loading well (with virtually no migration) in the same order. These factors precluded an assessment of the DNA photocleaving capacities of **3** and **4** but did point toward very strong DNA interactions that significantly altered the topological form of DNA.

Compounds **1** and **2** induced single-strand breaks in DNA when activated with visible light, which resulted in the slower migrating, nicked circular DNA (form II). Compound **2** was the more potent DNA-photodamaging agent but neither was considered particularly potent given that concentrations as high as $300 \mu\text{M}$ (drug-to-nucleotide ratio (r) = 10.5) did not

produce 100% form II DNA. Compounds **1** and **2** produced some DNA aggregation at the highest concentrations tested, but overall, the changes to plasmid DNA induced by **1** and **2** were less substantial than those observed for the more π -expansive compounds **3** and **4**.

When probed over the same concentration range as compounds **1** and **2**, metal complexes **3** and **4** acted as DNA condensation agents (Figure 7, lane 5). Notably, the DNA bands disappeared with higher concentrations of **3** or **4**, which suggests that ethidium cannot intercalate aggregated DNA effectively. In general, nonfluorescing DNA can be attributed to one or more of the following: (i) the DNA helix is significantly distorted (or made inaccessible) by metal-complex binding, preventing ethidium from binding, (ii) ethidium has been displaced from its binding sites by the metal complex, or (iii) the metal complex quenches ethidium fluorescence.

Experiments performed with metal complex concentrations from 1 to $50 \mu\text{M}$ ($r = 0.035\text{--}1.75$) showed traces of single-strand breaks (form II DNA) in parallel with mostly DNA aggregation/precipitation (Figures S13 and S14). For **3**, three forms of DNA were present when pUC19 plasmid was dosed with $18\text{--}27 \mu\text{M}$ metal complex: undamaged form I, nicked form II, and aggregates (form IV). At $30 \mu\text{M}$ MC, only form IV was observed on the gel, and higher concentrations of metal complex resulted in no fluorescence from ethidium bromide. The formation of DNA aggregates was confirmed by phase-contrast light microscopy (Figure S15), and precipitation was also visible by eye. Thus, we infer that DNA aggregation makes the DNA binding sites for ethidium inaccessible, resulting in no fluorescent bands on the gel. Compound **4** facilitated DNA aggregation/precipitation (Figure S15) at r values as low as 0.45, producing almost exclusively form IV DNA at metal complex concentrations greater than $20 \mu\text{M}$ ($r = 0.70$) with bands becoming invisible above $30 \mu\text{M}$ ($r = 1.05$). The disappearance of fluorescent bands with increasing concentrations of **3** or **4** alongside DNA aggregation/precipitation also occurred in the absence of a light trigger as demonstrated by lane 11 (Figure 7). It is possible that π -expansive cyclometalated complexes with fused systems of phenazine and longer interact with DNA through a templating effect that drives DNA aggregation followed by precipitation. It is known that chemical agents can cause DNA condensation by modifying electrostatic interactions between DNA segments, by modifying DNA-solvent interactions, by causing volume reductions of the helix, by causing local bending or distortion of the helical structure, or by combinations of these effects.⁶⁶ In the present series, the ability of the metal compound to facilitate DNA aggregation directly correlates with DNA intercalating power (where pbpn is predicted to be the best intercalating ligand because it has the largest π surface area), which in turn reflects the relative abilities of the compounds to act as DNA unwinders. Any further speculation on a definitive mechanism would require a detailed analysis of the DNA-metal complex structures, particularly with regard to whether they are of finite size and orderly morphology (true DNA condensation) or bulk aggregates of random size and shape.

We infer that the DNA aggregation/precipitation discerned for **4** by gel electrophoretic analysis does not account for the stark difference in dark and light cytotoxicity (PIs $> 1,400$ for **4** in some cases) measured for this π -expansive cyclometalated complex. Likewise, the ability to cause DNA aggregation/precipitation in the absence of light activation is not directly linked to dark cytotoxicity because the gel electrophoretic

patterns for **3** and **4** are strikingly similar, yet **3** is cytotoxic in the dark ($EC_{50} = 1\text{--}2 \mu\text{M}$) and **4** is not ($EC_{50} > 300 \mu\text{M}$). Others have demonstrated that increased hydrophobicity (positive log $P_{o/w}$ values) leads to increased cellular uptake, which in turn enhances cytotoxicity.³⁸ Following this logic, **4** should be the most lipophilic and therefore the most cytotoxic in the present series. However, the increased lipophilicity of the pbpn cyclometalating ligand could also facilitate the formation of extracellular π -stacked metal-complex assemblies with reduced cell penetration and dark cytotoxicity. The light trigger likely makes the cell membrane more permeable (known as photoactivated uptake^{67,68}) while simultaneously disrupting π -stacking interactions (through the formation of more highly polarized excited states). Factors other than cellular uptake (e.g., efflux, localization, redistribution, and metabolism) may also contribute to the dark cytotoxicity profiles for the Ru(II) cyclometalated complexes, and we are currently investigating a larger library of compounds to better understand this phenomenon.

ROS Detection. Plasmid DNA (in particular, changes to its gel mobility) serves as a convenient probe for detecting whether compounds can photodamage biological macromolecules in general, often via the production of ROS and other reactive intermediates that convert form I plasmid DNA to forms II or III. However, strong interactions between the more π -expansive cyclometalated complexes and DNA (vide supra) prevented a detailed analysis of any cleavage products. Therefore, an in vitro fluorescence-based assay for ROS detection was employed to scrutinize further the photactivity of **4**.

Given that $^1\text{O}_2$ production by the cyclometalated complexes was quite low ($\Phi_{\Delta} = 0.56\%$ for **4**), other reactive intermediates are likely responsible for the photocytotoxicity of this nondissociative cyclometalated system. In fact, the increased electron density on the metal in phpy^- complexes has been implicated in the cathodic shift of the $\text{Ru}^{\text{III}}/\text{Ru}^{\text{II}}$ potential³⁸ and could lead to direct photoreduction of biological macromolecules as well as dioxygen. To test the latter, we used the dihydroethidium (DHE) fluorescence assay for superoxide ($\text{O}_2^{\bullet-}$).⁶⁹

Briefly, cells were dosed with **4** ($10 \mu\text{M}$), washed, and then incubated with DHE ($3 \mu\text{M}$) for 15 min. The production of $\text{O}_2^{\bullet-}$ was inferred from the oxidation of the nonfluorescent DHE to ethidium, which emits red fluorescence ($\lambda_{\text{max}} = 610 \text{ nm}$) with blue-green excitation. Figure 8 shows the results

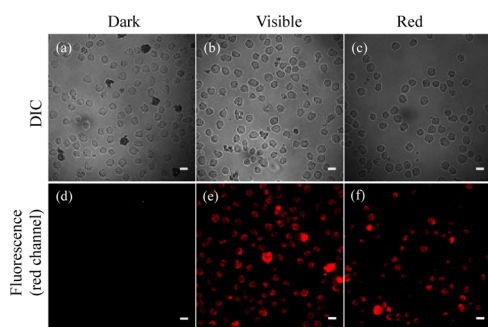


Figure 8. DIC (a–c) and fluorescence images (d–f) of HL-60 cells treated with **4** in the dark (left panel) or with a visible (middle panel) or red (right panel) light treatment (50 J cm^{-2}). Fluorescence emission was collected through a 510 nm long-pass filter. The scale bar corresponds to $10 \mu\text{m}$.

obtained when HL-60 cells were treated with **4** under various conditions (SK-MEL-28 results were similar). No fluorescent product was detected from cells that were exposed to **4** in the dark. Strikingly, ethidium emission was evident from all cells that were dosed with **4** followed by a visible (Figure 8e) or red (Figure 8f) light treatment. The intensity of red emission detected from visible and red light-treated cells correlated directly with the relative magnitudes of phototoxicity elicited by these two different light conditions (red light gave less potency). Consequently, $\text{O}_2^{\bullet-}$ may be a mediator of photocytotoxicity in addition to other mechanistic pathways that are influenced by cell uptake, efflux, localization, and relocation. Nevertheless, these results indicate that π -expansive cyclometalating compounds such as **4** may act as powerful photoreductants in cells.

3.3.3. Diagnostic Imaging. To probe whether ^1LC emission could serve as a diagnostic tool, compound **4** was incubated with SK-MEL-28 or HL-60 cells for 30 min prior to a dark or light treatment. Representative data taken 15 min post-treatment is shown for melanoma cells in Figure 9, where

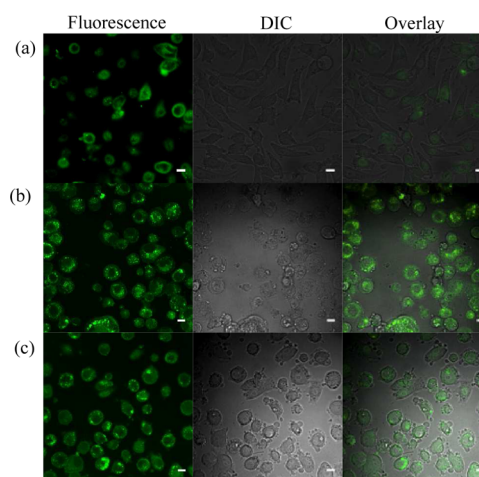


Figure 9. Comparison of the green fluorescence emitted from SK-MEL-28 cells dosed with **4** in the dark (a) or with a visible (b) or red (c) light treatment (50 J cm^{-2}). The scale bar corresponds to $10 \mu\text{m}$.

green emission is clearly visible from cells treated with the π -expansive cyclometalated compound under all three conditions (left panel, fluorescence). No red phosphorescence could be discerned, which is in agreement with the lack of red emission in steady-state luminescence measurements at room temperature.

Differential interference contrast (DIC) microscopy (center panel) was used to highlight cellular shape and morphology to ascertain the subcellular distribution of the photosensitizer before and after a light treatment. With no light treatment, compound **4** appeared to localize in the nucleus of SK-MEL-28 cells (Figure 9a). With observation at sublethal time points after a visible or red light dose (Figure 9b, c), **4** relocated to the cytoplasm concomitant with the gross changes in cellular morphology that accompany cell death pathways. These changes can be seen best by comparing the overlays of fluorescence and DIC images; fluorescence indicates where the compound is located within the DIC-imaged cell. The green signal was brightest in cell populations of the lowest viability (i.e., in those that received the most potent light treatment).

The polypyridyl cousin of **4**, **8**, did not produce any detectable green or red luminescence in cells, underscoring the importance of cyclometalation in providing an accessible ¹LC state for cellular imaging. Despite the fact that luminescence directly competes with photosensitization (and any other light-mediated cytotoxicity pathways) for excited-state deactivation, this radiative channel observed for **4** (and not **8**) did not compromise the photocytotoxicity for **4** in comparison to **8**. Both gave submicromolar light EC₅₀ values in both cell lines investigated. Therefore, one advantage afforded by the cyclometalating scaffold is the ability to turn potent photosensitizers into diagnostic agents.

4. SUMMARY AND CONCLUSIONS

Four organometallic Ru(II) compounds that systematically increase π -conjugation on the cyclometalating ligand were prepared and fully characterized. To our knowledge, this is the first investigation of tris-bidentate systems where π -expansion was probed on the cyclometalating framework rather than the diimine ligands. In agreement with previous reports of Ru(II) organometallics derived from non- π -expansive cyclometalating ligands, **1**–**3** did not act as potent light-responsive agents. Rather, they were extremely cytotoxic toward cancer cells in the dark, and light activation did not appreciably amplify this toxicity. Compound **4**, on the other hand, was completely nontoxic to cells in the dark, but was extremely phototoxic to cancer cells when activated with a moderate light treatment. This photoactivity was as potent as that previously reported for the related π -expansive Ru(II) polypyridyl system.

Despite the fact that the energy gap law might be invoked to explain red-shifted absorption, a lack of room-temperature phosphorescence, and low singlet oxygen quantum yields from cyclometalated Ru(II) complexes in this study, it does not compromise the photodynamic activity of **4** (which is comparable to **8**). In addition to excellent photocytotoxicity, compound **4** displayed intense green intracellular fluorescence that was not produced by the analogous Ru(II) polypyridyl complex **8**. This orthogonal functionality as a diagnostic tool makes cyclometalated **4** an attractive starting point for the investigation of whether triplet intraligand (³IL) excited states play a role in these cyclometalated systems that act as *theranostic* agents.

■ ASSOCIATED CONTENT

Supporting Information

The Supporting Information is available free of charge on the ACS Publications website at DOI: [10.1021/acs.inorgchem.5b01838](https://doi.org/10.1021/acs.inorgchem.5b01838).

1D ¹H and 2D ¹H–¹H COSY NMR spectra for cyclometalating ligands and their corresponding Ru(II) complexes, ¹³C NMR spectra for the metal complexes, narrow-range gel electrophoretic data, and microscopy images of DNA aggregates (PDF)

■ AUTHOR INFORMATION

Corresponding Author

*E-mail: sherri.mcfarland@acadiau.ca.

Notes

The authors declare no competing financial interest.

■ ACKNOWLEDGMENTS

We acknowledge financial support from the Natural Sciences and Engineering Council of Canada, the Canadian Foundation for Innovation, the Nova Scotia Research and Innovation Trust, and Acadia University.

■ REFERENCES

- (1) Bomben, P.; Robson, K.; Koivisto, B.; Berlinguette, C. *Coord. Chem. Rev.* **2012**, *256*, 1438–1450.
- (2) Alstrum-Acevedo, J. H.; Brennaman, M. K.; Meyer, T. J. *Inorg. Chem.* **2005**, *44*, 6802–6827.
- (3) Wu, A.; Yoo, D.; Lee, J.-K.; Rubner, M. F. *J. Am. Chem. Soc.* **1999**, *121*, 4883–4891.
- (4) McFarland, S. A.; Magde, D.; Finney, N. S. *Inorg. Chem.* **2005**, *44*, 4066–4076.
- (5) Lakowicz, J. R.; Malak, H.; Gryczynski, I.; Castellano, F. N.; Meyer, G. J. *Biospectroscopy* **1995**, *1*, 163–168.
- (6) McClure, B. A.; Rack, J. J. *Angew. Chem., Int. Ed.* **2009**, *48*, 8556–8558.
- (7) Kärkäs, M. D.; Verho, O.; Johnston, E. V.; Åkermark, B. *Chem. Rev.* **2014**, *114*, 11863–12001.
- (8) White, T. A.; Whitaker, B. N.; Brewer, K. J. *J. Am. Chem. Soc.* **2011**, *133*, 15332–15334.
- (9) Islangulov, R. R.; Kozlov, D. V.; Castellano, F. N. *Chem. Commun.* **2005**, 3776–3778.
- (10) Juris, A.; Balzani, V.; Barigelletti, F.; Campagna, S.; Belser, P.; von Zelewsky, A. *Coord. Chem. Rev.* **1988**, *84*, 85–277.
- (11) Lincoln, R.; Kohler, L.; Monroe, S.; Yin, H.; Stephenson, M.; Zong, R.; Chouai, A.; Dorsey, C.; Hennigar, R.; Thummel, R. P.; McFarland, S. A. *J. Am. Chem. Soc.* **2013**, *135*, 17161–17175.
- (12) Arenas, Y.; Monroe, S.; Shi, G.; Mandel, A.; McFarland, S.; Lilje, L. *Photodiagn. Photodyn. Ther.* **2013**, *10*, 615–625.
- (13) Shi, G.; Monroe, S.; Hennigar, R.; Colpitts, J.; Fong, J.; Kasimova, K.; Yin, H.; DeCoste, R.; Spencer, C.; Chamberlain, L.; Mandel, A.; Lilje, L.; McFarland, S. A. *Coord. Chem. Rev.* **2015**, *282–283*, 127–138.
- (14) Stephenson, M.; Reichardt, C.; Pinto, M.; Wächtler, M.; Sainuddin, T.; Shi, G.; Yin, H.; Monroe, S.; Sampson, E.; Dietzek, B.; McFarland, S. A. *J. Phys. Chem. A* **2014**, *118*, 10507–10521.
- (15) Yin, H.; Stephenson, M.; Gibson, J.; Sampson, E.; Shi, G.; Sainuddin, T.; Monroe, S.; McFarland, S. A. *Inorg. Chem.* **2014**, *53*, 4548–4559.
- (16) Monroe, S.; Scott, J.; Chouai, A.; Lincoln, R.; Zong, R.; Thummel, R. P.; McFarland, S. A. *Inorg. Chem.* **2010**, *49*, 2889–2900.
- (17) Holder, A. A.; Zigler, D. F.; Tarrago-Trani, M. T.; Storrer, B.; Brewer, K. J. *Inorg. Chem.* **2007**, *46*, 4760–4762.
- (18) Holder, A. A.; Swavey, S.; Brewer, K. J. *Inorg. Chem.* **2004**, *43*, 303–308.
- (19) Swavey, S.; Brewer, K. J. *Inorg. Chem.* **2002**, *41*, 6196–6198.
- (20) Higgins, S. L. H.; Brewer, K. J. *Angew. Chem., Int. Ed.* **2012**, *51*, 11420–11422.
- (21) Higgins, S. L. H.; Tucker, A. J.; Winkel, B. S. J.; Brewer, K. J. *Chem. Commun.* **2012**, *48*, 67–69.
- (22) Mari, C.; Gasser, G. *Chimia* **2015**, *69*, 176–181.
- (23) Mari, C.; Pierroz, V.; Ferrari, S.; Gasser, G. *Chem. Sci.* **2015**, *6*, 2660–2686.
- (24) Glazer, E. C. *Isr. J. Chem.* **2013**, *53*, 391–400.
- (25) Howerton, B. S.; Heidary, D. K.; Glazer, E. C. *J. Am. Chem. Soc.* **2012**, *134*, 8324–8327.
- (26) Wachter, E.; Howerton, B. S.; Hall, E. C.; Parkin, S.; Glazer, E. C. *Chem. Commun.* **2014**, *50*, 311–313.
- (27) Wachter, E.; Heidary, D. K.; Howerton, B. S.; Parkin, S.; Glazer, E. C. *Chem. Commun.* **2012**, *48*, 9649–9651.
- (28) Knoll, J. D.; Turro, C. *Coord. Chem. Rev.* **2015**, *282–283*, 110–126.
- (29) Sgambellone, M. A.; David, A.; Garner, R. N.; Dunbar, K. R.; Turro, C. *J. Am. Chem. Soc.* **2013**, *135*, 11274–11282.

- (30) Sears, R. B.; Joyce, L. E.; Ojaimi, M.; Gallucci, J. C.; Thummel, R. P.; Turro, C. *J. Inorg. Biochem.* **2013**, *121*, 77–87.
- (31) Ertl, C. D.; Ris, D. P.; Meier, S. C.; Constable, E. C.; Housecroft, C. E.; Neuburger, M.; Zampese, J. A. *Dalton Trans.* **2015**, *44*, 1557–1570.
- (32) Allen, F. H. *Acta Crystallogr., Sect. B: Struct. Sci.* **2002**, *58*, 380–388.
- (33) Muro-Small, M. L.; Yarnell, J. E.; McCusker, C. E.; Castellano, F. N. *Eur. J. Inorg. Chem.* **2012**, *2012*, 4004–4011.
- (34) Albani, B. A.; Peña, B.; Dunbar, K. R.; Turro, C. *Photochem. Photobiol. Sci.* **2014**, *13*, 272–280.
- (35) Bessho, T.; Yoneda, E.; Yum, J.-H.; Guglielmi, M.; Tavernelli, I.; Imai, H.; Rothlisberger, U.; Nazeeruddin, M. K.; Grätzel, M. *J. Am. Chem. Soc.* **2009**, *131*, 5930–5934.
- (36) Peña, B.; David, A.; Pavani, C.; Baptista, M. S.; Pellois, J.-P.; Turro, C.; Dunbar, K. R. *Organometallics* **2014**, *33*, 1100–1103.
- (37) Palmer, A. M.; Peña, B.; Sears, R. B.; Chen, O.; El Ojaimi, M.; Thummel, R. P.; Dunbar, K. R.; Turro, C. *Philos. Trans. R. Soc., A* **2013**, *371*, 20120135.
- (38) Huang, H.; Zhang, P.; Chen, H.; Ji, L.; Chao, H. *Chem. - Eur. J.* **2015**, *21*, 715–725.
- (39) Sullivan, B. P.; Salmon, D. J.; Meyer, T. J. *Inorg. Chem.* **1978**, *17*, 3334–3341.
- (40) Sun, Y.; Joyce, L. E.; Dickson, N. M.; Turro, C. *Chem. Commun.* **2010**, *46*, 6759–6761.
- (41) Schatzschneider, U.; Niesel, J.; Ott, I.; Gust, R.; Alborzina, H.; Wöfl, S. *ChemMedChem* **2008**, *3*, 1104–1109.
- (42) Friedman, A. E.; Chambron, J. C.; Sauvage, J. P.; Turro, N. J.; Barton, J. K. *J. Am. Chem. Soc.* **1990**, *112*, 4960–4962.
- (43) Zhou, Q.-X.; Lei, W.-H.; Chen, J.-R.; Li, C.; Hou, Y.-J.; Wang, X.-S.; Zhang, B.-W. *Chem. - Eur. J.* **2010**, *16*, 3157–3165.
- (44) Kosuge, T.; Senoo, A.; Ohru, H.; Muratsubaki, M. Azafluorene Derivative and Organic Light-Emitting Device Using the Derivative. US Patent 8,129,899 B1, March 6, 2012.
- (45) Delgadillo, A.; Romo, P.; Leiva, A. M.; Loeb, B. *Helv. Chim. Acta* **2003**, *86*, 2110–2120.
- (46) Sun, Y.; El Ojaimi, M.; Hammitt, R.; Thummel, R. P.; Turro, C. *J. Phys. Chem. B* **2010**, *114*, 14664–14670.
- (47) Koizumi, T.; Tomon, T.; Tanaka, K. *J. Organomet. Chem.* **2005**, *690*, 1258–1264.
- (48) Foxon, S. P.; Metcalfe, C.; Adams, H.; Webb, M.; Thomas, J. A. *Inorg. Chem.* **2007**, *46*, 409–416.
- (49) DeRosa, M. C.; Crutchley, R. J. *Coord. Chem. Rev.* **2002**, *233/234*, 351–371.
- (50) Croke, D. T.; Perrouault, L.; Sari, M. A.; Battioni, J.-P.; Mansuy, D.; Helene, C.; Le Doan, J. *J. Photochem. Photobiol., B* **1993**, *18*, 41–50.
- (51) Praseuth, D.; Gaudemer, A.; Verlhac, J.-B.; Kraljic, I.; Sissoëff, I.; Guillé, E. *Photochem. Photobiol.* **1986**, *44*, 717–724.
- (52) Robson, K. C. D.; Koivisto, B. D.; Yella, A.; Spornova, B.; Nazeeruddin, M. K.; Baumgartner, T.; Grätzel, M.; Berlinguette, C. P. *Inorg. Chem.* **2011**, *50*, 5494–5508.
- (53) Braven, J.; Hanson, R. W.; Smith, N. G. *J. Heterocycl. Chem.* **1995**, *32*, 1051–1055.
- (54) Saeki, K.; Tomomitsu, M.; Kawazoe, Y.; Momota, K.; Kimoto, H. *Chem. Pharm. Bull.* **1996**, *44*, 2254–2258.
- (55) Zelonka, R. A.; Baird, M. C. *Can. J. Chem.* **1972**, *50*, 3063–3072.
- (56) Bomben, P. G.; Gordon, T. J.; Schott, E.; Berlinguette, C. P. *Angew. Chem., Int. Ed.* **2011**, *50*, 10682–10685.
- (57) Fernandez, S.; Pfeffer, M.; Ritleng, V.; Sirlin, C. *Organometallics* **1999**, *18*, 2390–2394.
- (58) Constable, E. C.; Holmes, J. M. *J. Organomet. Chem.* **1986**, *301*, 203–208.
- (59) Reveco, P.; Medley, J. H.; Garber, A. R.; Bhacca, N. S.; Selbin, J. *Inorg. Chem.* **1985**, *24*, 1096–1099.
- (60) Sasaki, I.; Vendier, L.; Sournia-Saquet, A.; Lacroix, P. G. *Eur. J. Inorg. Chem.* **2006**, *2006*, 3294–3302.
- (61) Bomben, P. G.; Robson, K. C. D.; Sedach, P. A.; Berlinguette, C. P. *Inorg. Chem.* **2009**, *48*, 9631–9643.
- (62) Hissler, M.; Connick, W. B.; Geiger, D. K.; McGarrah, J. E.; Lipa, D.; Lachicotte, R. J.; Eisenberg, R. *Inorg. Chem.* **2000**, *39*, 447–457.
- (63) Goze, C.; Kozlov, D. V.; Tyson, D. S.; Ziessel, R.; Castellano, F. N. *New J. Chem.* **2003**, *27*, 1679–1683.
- (64) Sun, Y.; Joyce, L. E.; Dickson, N. M.; Turro, C. *Chem. Commun.* **2010**, *46*, 2426–2428.
- (65) Foxon, S. P.; Alamiry, M. A. H.; Walker, M. G.; Meijer, A. J. H. M.; Sazanovich, I. V.; Weinstein, J. A.; Thomas, J. A. *J. Phys. Chem. A* **2009**, *113*, 12754–12762.
- (66) Bloomfield, V. A. *Curr. Opin. Struct. Biol.* **1996**, *6*, 334–341.
- (67) Svensson, F. R.; Abrahamsson, M.; Strömberg, N.; Ewing, A. G.; Lincoln, P. *J. Phys. Chem. Lett.* **2011**, *2*, 397–401.
- (68) Svensson, F. R.; Matson, M.; Li, M.; Lincoln, P. *Biophys. Chem.* **2010**, *149*, 102–106.
- (69) Gomes, A.; Fernandes, E.; Lima, J. L. F. C. *J. Biochem. Biophys. Methods* **2005**, *65*, 45–80.